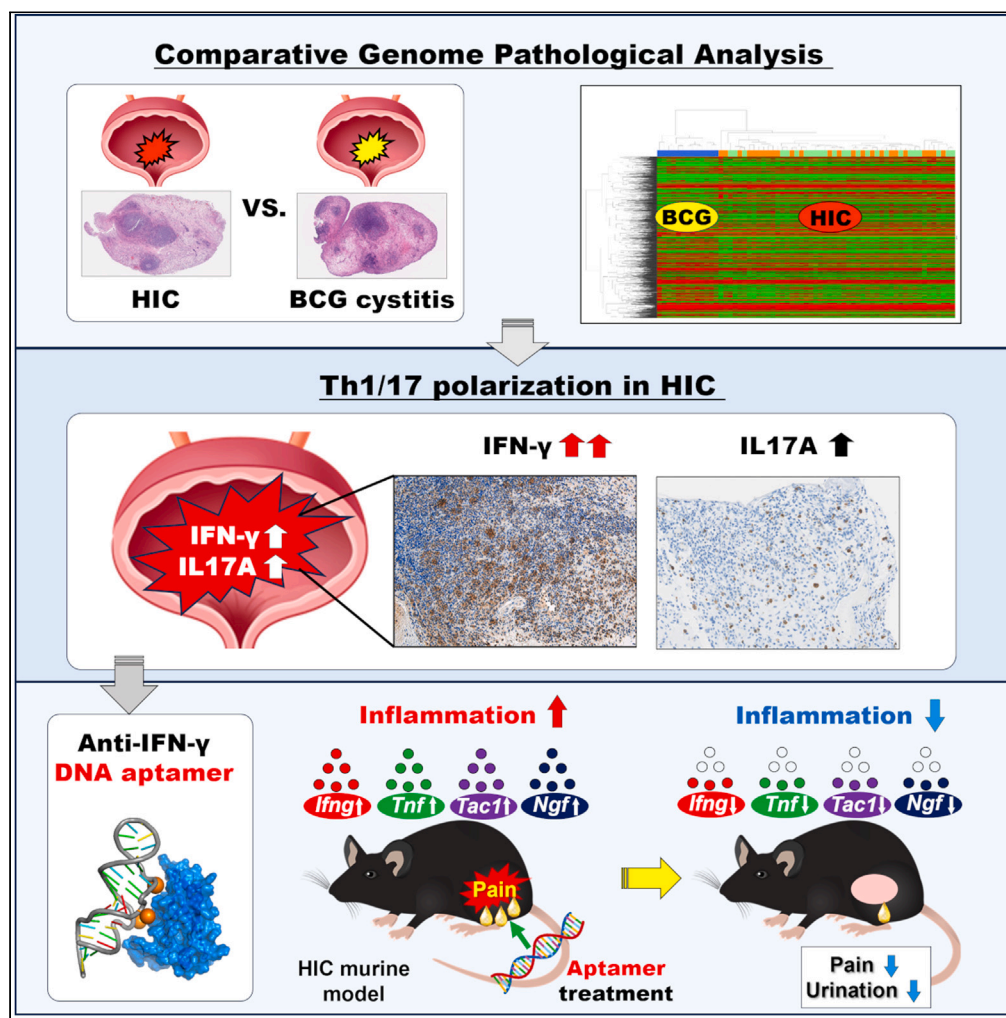


Article

# Th1/17 polarization and potential treatment by an anti-interferon- $\gamma$ DNA aptamer in Hunner-type interstitial cystitis



Yoshiyuki Akiyama, Kaori Harada, Jimpei Miyakawa, ..., Haruki Kume, Yukio Homma, Yi Luo

yoshiyuki-akiyama@uiowa.edu (Y.A.)  
m\_hori@tagcyx.com (M.H.)  
yi-luo@uiowa.edu (Y.L.)

**Highlights**

T helper 1/17 polarized immune responses characterize HIC inflammation

Enhanced cGAS-STING cytosolic DNA sensing pathway features HIC inflammation

Plasma cells are the key inflammatory infiltrates of the HIC bladder

Anti-IFN- $\gamma$  DNA aptamer shows the therapeutic efficacy in a murine model of HIC



## Article

Th1/17 polarization and potential treatment by an anti-interferon- $\gamma$  DNA aptamer in Hunner-type interstitial cystitis

Yoshiyuki Akiyama,<sup>1,2,8,9,\*</sup> Kaori Harada,<sup>3</sup> Jimpei Miyakawa,<sup>1</sup> Karl J. Kreder,<sup>2</sup> Michael A. O'Donnell,<sup>2</sup> Maeda Daichi,<sup>4</sup> Hiroto Katoh,<sup>5</sup> Miyuki Hori,<sup>3,\*</sup> Kensuke Owari,<sup>3</sup> Kazunobu Futami,<sup>3</sup> Shumpei Ishikawa,<sup>5</sup> Tetsuo Ushiku,<sup>6</sup> Haruki Kume,<sup>1</sup> Yukio Homma,<sup>1,7</sup> and Yi Luo<sup>2,\*</sup>

## SUMMARY

**Hunner-type interstitial cystitis (HIC) is a rare, enigmatic inflammatory disease of the urinary bladder with no curative treatments. In this study, we aimed to characterize the unique cellular and immunological factors specifically involved in HIC by comparing with cystitis induced by *Mycobacterium bovis* bacillus Calmette–Guérin, which presents similar clinicopathological features to HIC. Here, we show that T helper 1/17 +polarized immune responses accompanied by prominent overexpression of interferon (IFN)- $\gamma$ , enhanced cGAS-STING cytosolic DNA sensing pathway, and increased plasma cell infiltration are the characteristic inflammatory features in HIC bladder. Further, we developed a mouse anti-IFN- $\gamma$  DNA aptamer and observed that the intravesical instillation of the aptamer significantly ameliorated bladder inflammation, pelvic pain and voiding dysfunction in a recently developed murine HIC model with little migration into the blood. Our study provides the plausible basis for the clinical translation of the anti-IFN- $\gamma$  DNA aptamer in the treatment of human HIC.**

## INTRODUCTION

Hunner-type interstitial cystitis (HIC) is a rare, chronic debilitating inflammatory disease of the urinary bladder characterized by persistent bladder pain and lower urinary tract symptoms (LUTS), and the cystoscopic reddened mucosal lesion in the bladder, usually referred to as the Hunner lesion.<sup>1</sup> HIC falls under the interstitial cystitis/bladder pain syndrome (IC/BPS) symptom umbrella, that is clinically characterized by chronic pelvic/bladder pain in conjunction with LUTS such as urinary frequency and urgency.<sup>1,2</sup> The overall prevalence of IC/BPS is estimated to be 10.6 cases per 100,000 population worldwide, with a significantly higher prevalence in women than men.<sup>3</sup> HIC comprises 3.5%–50% of all IC/BPS cases.<sup>4</sup> To date, comprehensive understanding of the IC/BPS umbrella is still lacking due to its unknown etiology and low prevalence. However, growing evidence unveiled that HIC is a distinct inflammatory disease of the urinary bladder with severe pain and LUTS among the conditions classified as IC/BPS, while other forms of IC/BPS lacking Hunner lesions are non-inflammatory conditions accompanied by relatively moderate symptoms.<sup>4,5</sup> Currently, HIC is among the most intractable, devastating bladder disorders, with a severe impact on patients' quality of life (QOL).

The HIC bladder is known to present histological chronic inflammatory changes such as epithelial denudation, dense subepithelial inflammatory cell infiltration predominantly composed of lymphoplasmacytic and mast cells (frequently accompanied by lymphoid follicles/aggregates), stromal edema, and increased neovascularization.<sup>6</sup> The HIC bladder also manifests gene expression profiles associated with enhanced immune responses.<sup>5,7–11</sup> Based on this evidence, past studies implemented immunomodulatory therapies for patients with HIC and demonstrated that the systemic administration of Prednisone (a corticosteroid), Cyclosporine A (an immunosuppressive drug), and Certolizumab Pegol (an anti-tumor necrosis factor antibody) significantly improved symptoms in patients with HIC.<sup>12–14</sup> However, the current clinical guidelines for IC/BPS do not recommend proactive use of these immunomodulatory agents due to the concern on the systemic adverse effects that could surpass their clinical benefits, in addition to insufficient clinical evidence for these drugs.<sup>1,2,15</sup> Local therapy was then attempted to avert the systemic adverse events related to these agents. Although studies reported the treatment efficacy of the intravesical

<sup>1</sup>Department of Urology, Graduate School of Medicine, The University of Tokyo, Tokyo, Japan

<sup>2</sup>Department of Urology, University of Iowa, Iowa City, IA, USA

<sup>3</sup>TAGCyx Biotechnologies Inc., Tokyo, Japan

<sup>4</sup>Department of Molecular and Cellular Pathology, Graduate School of Medical Sciences, Kanazawa University, Kanazawa, Japan

<sup>5</sup>Department of Preventive Medicine, Graduate School of Medicine, The University of Tokyo, Tokyo, Japan

<sup>6</sup>Department of Pathology, Graduate School of Medicine, The University of Tokyo, Tokyo, Japan

<sup>7</sup>Department of Interstitial Cystitis Medicine, Faculty of Medicine, Kyorin University, Tokyo, Japan

<sup>8</sup>X (Formerly Twitter): @kei\_akiyama0405

<sup>9</sup>Lead contact

\*Correspondence: yoshiyuki-akiyama@uiowa.edu (Y.A.), m\_hori@tagcyx.com (M.H.), yi-luo@uiowa.edu (Y.L.)

<https://doi.org/10.1016/j.isci.2023.108262>



injection of steroid or dimethyl sulfoxide (DMSO) in patients with HIC,<sup>16,17</sup> the duration of the efficacy in both treatments was relatively short (less than 12 months) and most patients required the repeat injections to maintain the therapeutic effects.

Recent advances in the HIC research identified the upregulation of specific pro-inflammatory genes and molecules in patients with HIC, such as C-X-C motif chemokine receptor (CXCR) 3 and its ligands (CXCL9, CXCL10 and CXCL11),<sup>8,9,18</sup> C-C motif chemokine ligand 2 (CCL2),<sup>19</sup> Toll-like receptor (TLR) 7,<sup>10</sup> tumor necrosis factor (TNF) family B-cell-activating factor (BAFF),<sup>5</sup> vascular endothelial growth factor (VEGF),<sup>5</sup> hypoxia-inducible factor (HIF) 1  $\alpha$ ,<sup>20</sup> TNF- $\alpha$ ,<sup>9</sup> interferon (IFN)- $\gamma$ ,<sup>9</sup> interleukin (IL)-6,<sup>11</sup> IL-10,<sup>11</sup> and IL-17.<sup>5,11</sup> These molecules, however, were mainly gained by comparisons between HIC and healthy bladders or bladders with non-inflammatory conditions, such as overactive bladder, IC/BPS without Hunner lesions, or benign prostatic hyperplasia. Hence, it is unclear whether these candidates truly play a key role in HIC inflammation. To date, novel therapies targeting these inflammatory mediators have not yet been developed. To identify the specific factors contributing to HIC pathogenesis, a comparison with inflammatory conditions of the urinary bladder that resembles HIC is necessary.

In the present study, we aimed to characterize the cellular and molecular factors specifically involved in HIC by comparing with the cystitis induced by the bladder instillation of *Mycobacterium bovis* bacillus Calmette–Guérin (BCG), a clinicopathologically HIC-similar cystitis with known pathogenesis. BCG cystitis shows histological changes similar to those of HIC, such as dense subepithelial lymphocytic infiltration with the frequent formation of lymphoid follicles or aggregates, epithelial denudation, increased neovascularization, stromal edema and fibrosis.<sup>21,22</sup> In addition, patients with BCG cystitis frequently presents similar clinical characteristics to patients with HIC such as persistent pelvic pain, irritable LUTS (e.g., urinary frequency and urgency), and a reduced bladder capacity that could ultimately lead to bladder contraction.<sup>23</sup> Furthermore, intravesical instillation of BCG Tokyo strain, which was used in this study, induces pro-inflammatory cytokines skewed toward T helper (Th) 1 immune responses such as IFN- $\gamma$ , IL-2, IL-12 and TNF in the bladder,<sup>24</sup> providing a similar local environment of immune reactions to HIC.<sup>5,20</sup> Thus, BCG cystitis presents a wide range of clinicopathological similarities with HIC, which are rarely seen in other chronic inflammatory conditions of the bladder such as chronic bacterial cystitis and follicular cystitis.<sup>22</sup> Therefore, BCG cystitis provides an ideal counterpart to HIC, allowing more specific analysis of HIC in terms of gene expression and biological activity. In addition, we also aimed to utilize a DNA aptamer as an alternative therapeutic agent for a protein-based antibody intravesical therapy, as a DNA-based aptamer has higher structural stability, binding affinity and avidity to its target molecules than a protein-based antibody. Also, a DNA-based aptamer generally lacks immunogenicity and can be washed out swiftly from the blood circulation system.<sup>25</sup>

Here, we show that Th 1/17-polarized immune responses accompanied by prominent overexpression of IFN- $\gamma$ , enhanced cGAS-STING cytosolic DNA sensing pathway, and increased plasma cell infiltration are the characteristic inflammatory features of the HIC bladder. We also show that the intravesical instillation of an anti-IFN- $\gamma$  DNA aptamer significantly ameliorated bladder inflammation, pelvic nociception and voiding dysfunction in a murine model of HIC, providing a potential novel therapy for human HIC.

## RESULTS

### Characteristics of the study participants

Patient demographics are shown in Table 1. The study cohort comprised 25 patients with HIC (23 females) and 13 patients with BCG cystitis (5 females), who were recruited at The University of Tokyo Hospital between 2016 and 2019. The diagnosis of HIC was made according to the East Asian clinical guidelines and the International Society for the Study of IC/BPS (ESSIC) criteria.<sup>1,26</sup> The diagnosis of BCG-related chronic cystitis was made based on histological evidence of granulation tissue, epithelial denudation, increased neovascularization, stromal edema and fibrosis, and dense subepithelial lymphocytic infiltration with the frequent formation of lymphoid follicles or aggregates, besides a negative urine culture (indicating that the number of cultured microbiomes less than  $10^3$  CFU/mL). All 13 participants in the BCG group had previously been diagnosed with primary intermediate- or high-risk non-muscle invasive bladder cancer (NMIBC) including carcinoma *in situ* (CIS), Ta, and T1 stages, classified according to the European Association of Urology (EAU) guidelines<sup>27</sup> and undergone transurethral resection of the tumor, followed by adjuvant prophylactic or therapeutic intravesical instillation of BCG (Tokyo 172 strain, 80mg; Nihon BCG, Tokyo, Japan). After BCG therapy, screening bladder biopsies were taken when patients showed irregular-looking and reddened bladder mucosal lesions at routine follow-up cystoscopy, with urine cytology class III (5 patients) or negative cytology (8 patients), and histologically examined for the recurrent malignancy.

One cold-cup biopsy sample was obtained from the reddened mucosal flat lesions resembling Hunner lesions (Figure S1) in patients of the BCG group, which was subsequently diagnosed as BCG cystitis and proven pathologically to be nonmalignant. At biopsy, all patients of the BCG group had no concomitant bladder cancer. In patients with HIC, two cold-cup biopsy samples were obtained from the Hunner lesion and background non-Hunner lesion area (one sample each). All patients in both groups had no concomitant, apparent urinary tract infection, as indicated by negative urine culture in conjunction with the absence of pyuria.

The mean duration of illness in patients with HIC prior to biopsy was  $5.2 \pm 4.6$  years, and the mean duration from the last BCG instillation to biopsy in patients with BCG cystitis was  $2.3 \pm 2.0$  years. The mean ages at biopsy were significantly younger in patients with HIC than BCG cystitis ( $66.0 \pm 11.8$  vs.  $74.8 \pm 4.7$ ,  $p < 0.05$ ). Patients with HIC had worse symptom severity than patients with BCG cystitis as measured by O’Leary and Sant’s symptom index and problem index (OSSI/PI) ( $15.4 \pm 3.0$  vs.  $7.1 \pm 4.7$ ,  $p < 0.001$  and  $13.3 \pm 2.6$  vs.  $4.2 \pm 3.2$ ,  $p < 0.001$ , respectively).<sup>28</sup> The pain intensity evaluated by an 11-point numerical scale was also significantly higher in patients with HIC than BCG cystitis ( $8.0 \pm 1.7$  vs.  $1.2 \pm 2.7$ ,  $p < 0.001$ ). Meanwhile, QOL scores assessed by a 7-grade, with 0 indicating excellent and 6 indicating terrible, were equivalently worse between the two groups ( $5.7 \pm 0.9$  vs.  $5.3 \pm 1.7$ ,  $p = 0.86$ ). The average and maximum voided volumes were comparably reduced in patients with HIC and BCG cystitis ( $102.9 \pm 51.7$  vs.  $109.1 \pm 60.3$ ,  $p = 0.82$  and  $168.0 \pm 90.5$  mL vs.  $184.5 \pm 99.6$ ,  $p = 0.70$ , respectively).

**Table 1. Demographics of the study subjects**

	HIC	BCG cystitis	p value <sup>a</sup>
No. (male/female)	25 (2/23)	13 (8/5)	<0.001 <sup>b</sup>
Mean age at biopsy (years)	66.0 ± 11.8 [37–80] <sup>c</sup>	74.8 ± 6.9 [64–85]	<0.05
OSSI	15.4 ± 3.0 [11–20]	7.1 ± 4.7 [3–18]	<0.001
OSPI	13.3 ± 2.6 [8–16]	4.2 ± 3.2 [1–11]	<0.001
Pain intensity <sup>d</sup>	8.0 ± 1.7 [4–10]	1.2 ± 2.7 [0–7]	<0.001
QOL score <sup>e</sup>	5.7 ± 0.9 [2–6]	5.3 ± 1.7 [4–6]	0.86
Daytime frequency	14.7 ± 5.2 [4–27]	9.4 ± 3.2 [5–15]	<0.05
Nocturia	3.8 ± 1.8 [0–7]	1.9 ± 1.5 [0–4]	<0.01
Average voided volume (mL)	102.9 ± 51.7 [31–221]	109.1 ± 60.3 [60–250]	0.82
Maximum voided volume (mL)	168.0 ± 90.5 [50–420]	184.5 ± 99.6 [100–400]	0.70
Maximum bladder capacity at hydrodistension (mL)	394.0 ± 155.0 [200–700]	NA	–

NA, not applicable; BCG, bacillus Calmette–Guérin; HIC, Hunner-type interstitial cystitis; OSSI/OSPI, O’Leary and Sant symptom index/O’Leary and Sant problem index; QOL, quality of life.

<sup>a</sup>Wilcoxon rank-sum test for continuous variables or Fisher’s exact test for categorical variables.

<sup>b</sup>Statistical significance,  $p < 0.05$ .

<sup>c</sup>Mean ± SD [range].

<sup>d</sup>Assessed using an 11-point pain intensity numerical rating scale from 0 (“no pain”) to 10 (“the worst pain ever”).

<sup>e</sup>Assessed on a 7-grade quality of life (QOL) scale derived from the International Prostate Symptom Score, with 0 indicating “excellent” and 6 indicating “terrible.”

### Hunner-type interstitial cystitis and bacillus Calmette–Guérin cystitis bladders exhibit distinct gene expression profiles

Initially, we sequenced mRNA extracted from bladder biopsy samples of HIC (both Hunner lesion areas and non-Hunner lesion areas) and BCG cystitis. The total and sample-by-sample read counts are shown in [Table S1](#).

Of 14,554 genes detected in all samples, 6,641 were differentially expressed in pairwise comparisons among the three groups (Hunner lesions in HIC, non-Hunner lesion areas in HIC and BCG cystitis) ([Table S2](#)). Given the previously revealed pancystitic nature of HIC that Hunner lesions and non-Hunner lesion areas manifest similar gene expression profiles and histological features,<sup>5,6,8,29</sup> both differentially expressed genes (DEGs) between Hunner lesions and BCG cystitis and DEGs between non-Hunner lesion areas and BCG cystitis were used for searching HIC-specific DEGs in further analyses. Then, a Venn diagram constructed using the DEGs that were either significantly upregulated or significantly downregulated in both Hunner lesions and non-Hunner lesion areas compared to BCG cystitis identified 3,682 HIC-specific DEGs, including 1,718 upregulated and 1,964 downregulated genes ([Table S3](#)). Hierarchical clustering analysis using these HIC-specific DEGs yielded two distinct clusters, corresponding to HIC and BCG cystitis groups separately ([Figure 1](#)), indicating distinct gene expression profiles between HIC (Hunner lesion and/or non-Hunner lesions area) and BCG cystitis.

### Biological pathways involved in innate and adaptive immune responses are upregulated in Hunner-type interstitial cystitis

The identified HIC-specific DEGs were subjected to Gene Ontology (GO)/GO Slim analyses and Kyoto Encyclopedia of Genes and Genomes (KEGG) pathway enrichment analysis. The results of the GO and GO Slim analyses of the 3,682 HIC-specific DEGs are shown in [Figure S2](#) and [Tables S4](#), [S5](#), and [S6](#). The GO Slim analysis revealed that the HIC-specific upregulated DEGs were associated with the biological process terms “biological process” and “immune system process”, the cellular component terms “cytosol” and “cytoplasm”, and the molecular function terms “enzyme binding” and “DNA binding” ([Figures S2A–S2C](#)). The HIC-specific downregulated DEGs were associated with the biological process terms “biological process” and “biosynthetic process”, the cellular component terms “cellular component” and “nucleus”, and the molecular function terms “molecular function” and “ion binding” ([Figures S2D–S2F](#)). The KEGG pathway analysis identified 111 significantly upregulated pathways in HIC including “Natural killer cell-mediated cytotoxicity”, “Antigen processing and presentation”, “Th17 cell differentiation”, “IL-17 signaling pathway”, “T cell receptor signaling pathway”, “B cell receptor signaling pathway”, “Toll-like receptor signaling pathway” and “Cytosolic DNA-sensing pathway.” The KEGG pathway analysis also identified 64 significantly downregulated pathways in HIC including “Ribosome”, “Peroxisome” and “Metabolic pathways” ([Table S7](#)). These results suggest that biological pathways involved in innate and adaptive immune responses, especially those polarized toward the Th1/17 axis, are upregulated in the HIC bladder compared to the BCG cystitis bladder.

### Increased expression levels of genes involved in Th1/17-polarized immune responses in Hunner-type interstitial cystitis

Next, we performed quantitative PCR analysis of the bladder biopsy samples of HIC and BCG cystitis to analyze the mRNA levels of genes that play a key role in innate and Th1/2/17-mediated adaptive immune responses, including *IL2*, *IL4*, *IL6*, *IL10*, *IL12 A/B*, *IL17A*, *IL22*, *IL23R*, *HIF1A*, *IFNA17*, *IFNB1*, *IFNG*, *TNF*, transforming growth factor  $\beta$ 1 (*TGFB1*), *TBX21*, *GATA3*, *RORC*, *CTLA4*, cyclic GMP-AMP (cGAMP) synthase (*CGAS*), and stimulator of interferon genes (*STING1*). Compared to BCG cystitis bladders, the HIC bladders exhibited significantly

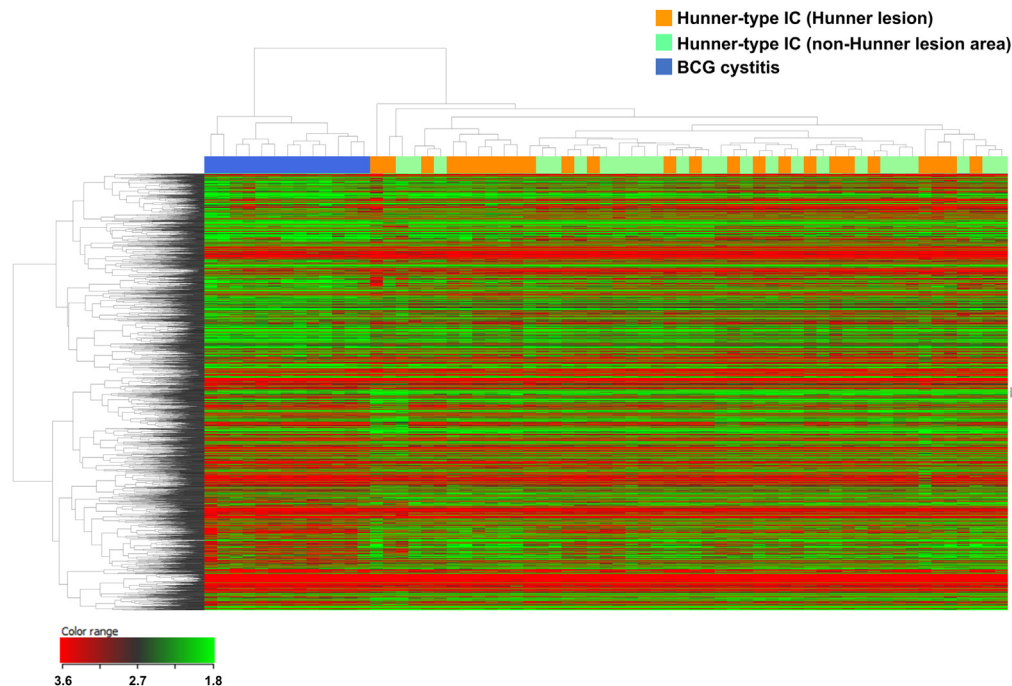


**Figure 1. Hierarchical clustering analysis of bladder DEGs indicates distinct gene expression patterns between HIC and BCG groups**

A heatmap generated by hierarchical clustering analysis of DEGs among Hunner lesions, non-Hunner lesion areas, and BCG cystitis. Red: high relative expression; green: low relative expression. See also [Table S2](#).

increased mRNA expression of *IL17A*, *IFNG*, *TBX21*, *RORC*, *CGAS* and *STING*, highlighted by concomitantly reduced *GATA3* mRNA expression ([Figure 2A](#)). Moreover, the ratios of Th1/Th2 (*TBX21/GATA3* and *IFNG/GATA3*) and Th17/Th2 (*RORC/GATA3* and *IL17A/GATA3*) marker genes were significantly higher in the HIC bladders than in the BCG cystitis bladders ([Figure 2B](#)), indicating the importance of Th1/17-polarized immune responses in HIC inflammation.

### Intensified CD138, IFN- $\gamma$ , IL-17A, cyclic GMP-AMP (cGAMP) synthase and stimulator of interferon genes positivity in Hunner-type interstitial cystitis

Then, we performed histological analysis of the bladder biopsy samples of HIC and BCG cystitis to compare the degree of chronic inflammation and evaluate the Th1/17 immune polarization at the cellular and protein levels in both cystitis types. First, we observed similar chronic inflammatory changes in HIC and BCG cystitis by hematoxylin and eosin (H&E) staining, such as subepithelial dense mononuclear cell infiltration with the frequent formation of lymphoid follicles or aggregates, epithelial denudation, increased neovascularization, stromal edema and fibrosis ([Figure 3A](#)). Next, we performed digital immunohistochemical quantification for CD3<sup>+</sup>, CD4<sup>+</sup>, CD8<sup>+</sup>, CD20<sup>+</sup>, CD138<sup>+</sup>, cytokeratin<sup>+</sup>, forkhead box P3 (FOXP3)<sup>+</sup>, IL-17A<sup>+</sup>, and mast cell tryptase (MCT)<sup>+</sup>-positivity as described previously ([STAR Methods](#)).<sup>6,29</sup> We observed comparable lymphoplasmacytic (sum of CD3<sup>+</sup>, CD20<sup>+</sup> and CD138<sup>+</sup>-positive cells) and MCT-positive mast cell densities, which accounted for the majority of subepithelial inflammatory infiltrates, in both cystitis ([Figure 3A](#)). We also observed similar CD4<sup>+</sup>, CD8<sup>+</sup> and FOXP3<sup>+</sup>-positive T cell densities, CD4/CD8 ratio, and epithelial/specimen ratio (proportion of cytokeratin-positive area per whole tissue sample area) in both cystitis types ([Figures 3A–3C](#)). However, the IL-17A<sup>+</sup>-positive cell density and plasma cell ratio (plasma cell density/lymphoplasmacytic cell density) were significantly higher in HIC than BCG cystitis ([Figures 3B and 3C](#)). The ratio of IL-17A<sup>+</sup>/FOXP3<sup>+</sup>-positive cell densities was also significantly higher in HIC (non-Hunner lesion areas) than BCG cystitis ([Figure 3C](#)). Due to their background stromal immunoreactivity along with the cellular positivity, digital quantitative analysis was not applied for IFN- $\gamma$ , cGAS- and STING-positivity. Instead, the IHC staining intensity for each of these three proteins was evaluated based on the cellular (and stromal for IFN- $\gamma$ ) immunoreactive intensity as follows: negative, mild, moderate and strong, as described elsewhere.<sup>30</sup> Specimens with a negative or mild intensity were defined as having low immunoreactivity, and those with a moderate or strong intensity were defined as having high immunoreactivity. The immunoreactivities of cGAS and STING were detected in subepithelial mononuclear cells, and they were significantly intensive in HIC than BCG cystitis ([Figures 4 and 5A](#)). The immunoreactivity of IFN- $\gamma$  was detected in both subepithelial mononuclear cells and stroma, and it was much more intensive in HIC than BCG cystitis ([Figures 4 and 5B](#)). These results indicate the potential of IFN- $\gamma$  as a therapeutic target for HIC and the importance of increased Th17 and plasma cell infiltrations as well as enhanced cGAS-STING cytosolic DNA sensing pathway in HIC inflammation.

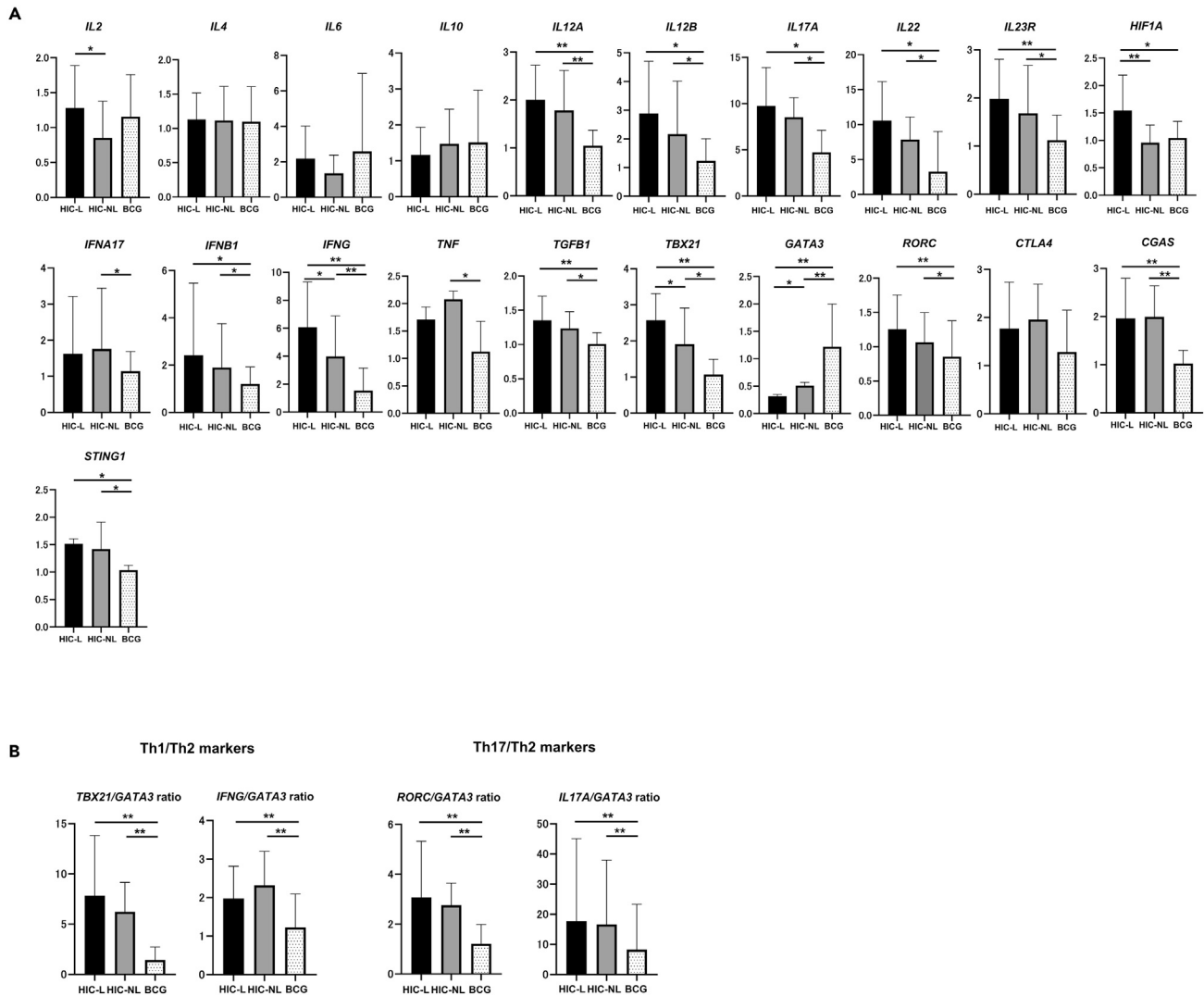


**Figure 2. Bladder quantitative PCR analysis shows increased mRNA levels of pro-Th1/17, cGAS and STING in HIC**

(A) Quantitative PCR analysis of *IL2*, *IL4*, *IL6*, *IL10*, *IL12A*, *IL12B*, *IL17A*, *IL22*, *IL23R*, *HIF1A*, *IFNA17*, *IFNB1*, *IFNG*, *TNF*, *TGFB1*, *TBX21*, *GATA3*, *RORC*, *CTLA4*, *CGAS*, and *STING1* in the bladder samples of Hunner lesion areas (HIC-L), non-Hunner lesion areas (HIC-NL), and BCG cystitis.

The expression level of each gene is reported relative to that of *IPO8*. Data shown are the mean  $\pm$  SD relative gene expressions.

(B) Ratios of Th1/Th2 markers (left two graphs) and Th17/Th2 markers (right two graphs) in the bladder samples of Hunner lesion areas (HIC-L), non-Hunner lesion areas (HIC-NL), and BCG cystitis. Data are shown as mean  $\pm$  SD.

\* $p < 0.05$  and \*\* $p < 0.01$ , statistically significant by Steel-Dwass test.

### Generation, characterization and pharmacokinetic study of a mouse anti-interferon- $\gamma$ DNA aptamer

Based on the results of the human study above, we next tested the effect of IFN- $\gamma$  blockade in a mouse HIC model to explore if targeting IFN- $\gamma$  can be a potential therapy for human HIC. To this end, we utilized an anti-IFN- $\gamma$  DNA aptamer as a therapeutic agent. The DNA-based aptamer has higher stability in structure and smaller molecular size compared to a protein-based antibody, which enables the aptamer to penetrate the bladder epithelium and bind to targets, with high affinity and specificity.<sup>25</sup> In the present study, we developed an anti-mouse IFN- $\gamma$  DNA aptamer using the systematic evolution of ligands by exponential enrichment (SELEX) method using our proprietary unnatural base pair technology platform as described previously (STAR Methods).<sup>31</sup> Through the SELEX selection, we obtained two candidate sequences for a mouse IFN- $\gamma$  aptamer, mIFN $\gamma$ 5-1mh and mIFN $\gamma$ 6-1mh (Table S8). The binding affinities between each candidate sequence and mouse IFN- $\gamma$  were determined by surface plasmon resonance (SPR) analysis. The inhibitory activity of each candidate sequence was determined by flow cytometric analysis of IFN- $\gamma$ -induced signal transducer and activator of transcription1 (STAT1) phosphorylation in the presence of the aptamers. Consequently, mIFN $\gamma$ 6-1mh was selected as the lead candidate aptamer for the evaluation, as it demonstrated the higher binding affinity for mouse IFN- $\gamma$  ( $K_D = 2.47$  nM) (Figure S3A) and higher inhibitory activity on IFN- $\gamma$ -induced STAT1 phosphorylation (Figure S3B).

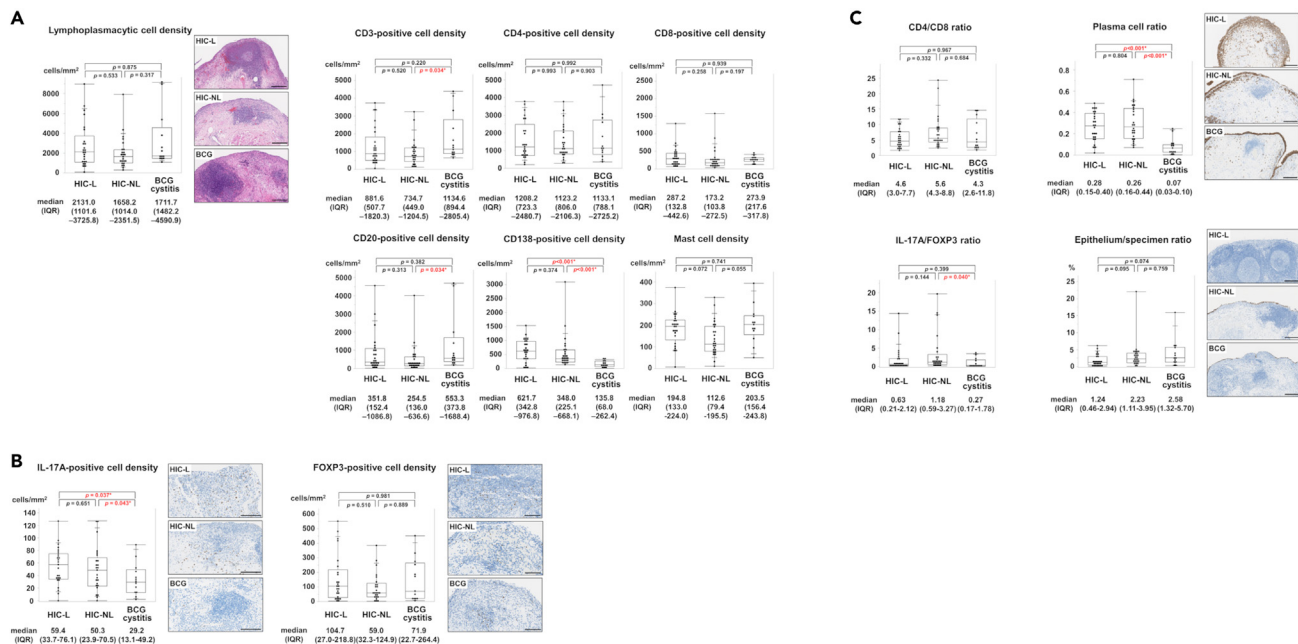


**Figure 3. Bladder immunohistochemical quantification demonstrates comparable lymphoplasmacytic and mast cell densities between HIC and BCG cystitis but higher IL-17A-positive cell density and plasma cell ratio in HIC**

(A) Densities of lymphoplasmacytic (the sum of CD3<sup>+</sup>, CD20<sup>+</sup> and CD138<sup>+</sup>-positive cells) and CD4<sup>+</sup>, CD8<sup>+</sup>, and mast cell tryptase-positive cells. Representative hematoxylin and eosin staining images of the Hunner lesion areas (HIC-L), non-Hunner lesion areas (HIC-NL), and BCG cystitis are shown along with the lymphoplasmacytic cell density diagram. (scale bar: 250  $\mu$ m).

(B) Densities of IL-17A- and FOXP3-positive cells with representative immunohistochemical images. (scale bar: 200  $\mu$ m in IL-17A, 100  $\mu$ m in FOXP3).

(C) The ratios of CD4-positivity to CD8-positivity, CD138-positivity to the sum of CD3<sup>+</sup>, CD20<sup>+</sup> and CD138<sup>+</sup>-positivity ("Plasma cell ratio"), IL-17A-positivity to FOXP3-positivity, and epithelial area to whole specimen area, with representative immunohistochemical images. (scale bar: 250  $\mu$ m).

Values are expressed as the median (interquartile range).

\* $p < 0.05$ , statistically significant by Steel–Dwass test.

A pharmacokinetic study on the intravesical instillation of mIFN $\gamma$ -1mh (10 nmol/bladder) in female CD-1 mice showed that mIFN $\gamma$ -1mh was detected in the bladder tissue and plasma samples 10 min after the intravesical instillation (Table 2). By 3 h, >99% of the aptamer was washed out from both bladder tissue and plasma samples.

### Intravesical instillation of mIFN $\gamma$ -1mh significantly reduced bladder inflammation, pelvic nociceptive response, and urinary frequency in the Hunner-type interstitial cystitis-like URO-OVA cystitis model

Then, to test the feasibility of mIFN $\gamma$ -1mh as a therapy for HIC, we evaluated the aptamer using our recently developed murine model of HIC.<sup>32</sup> This model reproduces many histological and clinical correlates of human HIC, such as dense mononuclear cell infiltrates predominantly composed of T and B lymphocytes, increased pelvic pain and voiding dysfunction, as well as elevated mRNA levels of IFN- $\gamma$  and other inflammatory/pain factors.

In this model, HIC-like bladder inflammation was induced in URO-OVA mice, a transgenic line that expresses the well-defined model antigen ovalbumin (OVA) as a self-antigen on the bladder epithelium,<sup>33</sup> by adoptive transfer of OVA-primed splenocytes from C57BL/6 mice (Figure 6A) as previously described.<sup>32</sup> Here, beginning immediately after cystitis induction on day 0, the cystitis-induced mice were intravesically treated with phosphate-buffered saline (PBS, 100  $\mu$ L, n = 5) or mIFN $\gamma$ -1mh (10 nmol in 100  $\mu$ L PBS, n = 7) every other day for a total of 12 times. The mice were then euthanized two days after the last treatment, and the samples (serum and bladder) were collected for analysis. Sex- and age-matched cystitis-uninduced URO-OVA mice (i.e., received no OVA-primed splenocyte transfer, n = 5) were included for comparison.

Bladder histological analysis showed that three of the five PBS-treated cystitis mice exhibited remarkable bladder inflammation that manifested dense mononuclear cell infiltration, increased vascularity, mucosal hyperemia, and interstitial edema compared with the cystitis-uninduced mice (Figures 6B; Table 3). Conversely, all seven mIFN $\gamma$ -1mh-treated cystitis mice exhibited no or minimal bladder inflammation. Along with the histological changes, the bladders from PBS-treated cystitis mice exhibited significantly increased mRNA levels of *Ifng*, *Tnf*, *Tac1* (tachykinin-1, also referred to as substance P precursor), and *Ngf* (nerve growth factor) compared with the bladders from cystitis-uninduced mice (Figure 6C,  $p < 0.001$  for all four molecules), while the bladders from mIFN $\gamma$ -1mh-treated cystitis mice exhibited significantly reduced levels of these mRNAs compared with the bladders from PBS-treated cystitis mice. (Figure 6C,  $p < 0.001$  for *Ifng* and  $p < 0.01$  for the three other molecules).

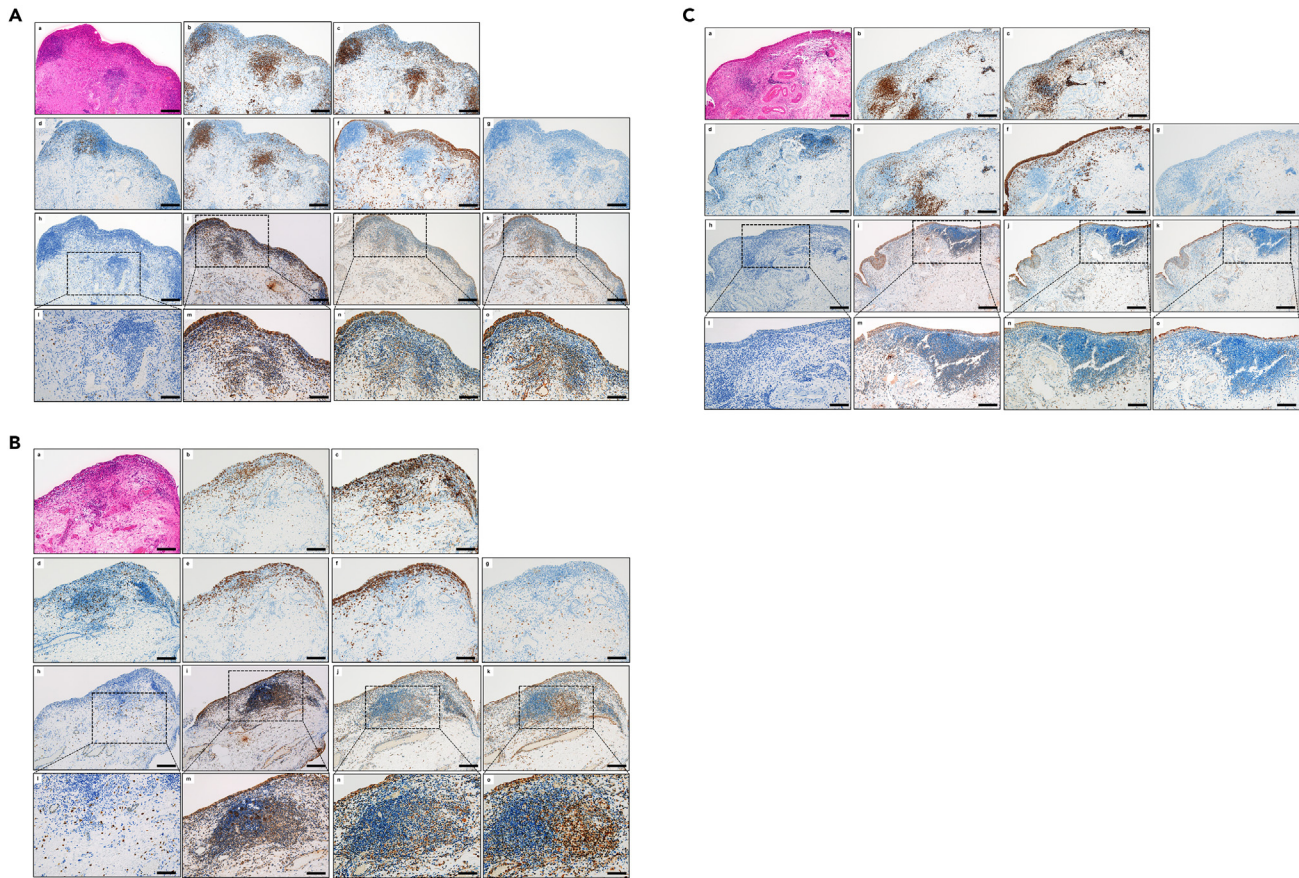


**Figure 4. Representative images of serial sections of the bladders from patients with HIC or BCG cystitis evaluated by hematoxylin and eosin staining or immunohistochemical staining with antibodies against CD3, CD4, CD8, CD20, CD138, mast cell tryptase, IL-17A, IFN- $\gamma$ , cGAS, and STING**

(A) Hunner lesion of HIC.

(B) Non-Hunner lesion area of HIC.

(C) BCG cystitis.

(a) Hematoxylin and eosin staining.

(b–k) Immunohistochemistry: (b) CD3, (c) CD4, (d) CD8, (e) CD20, (f) CD138, (g) mast cell tryptase, (h) IL-17A, (i) IFN- $\gamma$ , (j) cGAS, (k) STING (scale bar: 200  $\mu$ m).

(l–o) Enlarged images of the areas indicated by the rectangular boxes in h–k, respectively (scale bar: 100  $\mu$ m).

In addition to bladder inflammation, we evaluated the intravesical IFN- $\gamma$  blockade on pelvic nociception and voiding behavior in the cystitis mice. Previously, we demonstrated increases in both pelvic nociception and urinary frequency in this model.<sup>32</sup> Likewise, in this study, the PBS-treated cystitis mice exhibited decreased sensory thresholds for pelvic nociception on days 8, 15 and 22 after cystitis induction (Figure 6D). However, intravesical instillation of mIFN $\gamma$ 6-1mh significantly reversed the decreased sensory threshold for pelvic nociception compared with the intravesical instillation of PBS in the cystitis mice ( $p < 0.05$  on day 8 and  $p < 0.01$  on days 15 and 22) (Figure 6D). Similarly, PBS-treated cystitis mice exhibited increased urinary frequency at weeks 1, 2 and 3 after cystitis induction, while the intravesical instillation of mIFN $\gamma$ 6-1mh completely reversed this increase in urinary frequency ( $p = 0.061$  at week 1 and  $p < 0.05$  at week 2) (Figure 6E). Furthermore, intravesical instillation of mIFN $\gamma$ 6-1mh led to a trend toward increased voided volume per micturition (at weeks 1 and 2) in the cystitis mice (Figure S4). In addition, we observed that the mean aptamer concentration in serum, measured by quantitative PCR analysis, was very low ( $0.89 \pm 0.42$  p.m.), which was consistent with the pharmacokinetic findings for CD-1 mice treated intravesically with the same aptamer (described above). Our results indicated that intravesical blockade of IFN- $\gamma$  by mIFN $\gamma$ 6-1mh effectively ameliorated HIC-like bladder inflammation and symptoms with the minimal migration of the aptamer into the serum in a validated cystitis murine model, suggesting the potential utility of the anti-IFN- $\gamma$  aptamer strategy for the treatment of human HIC.

### **Intravesical instillation of mIFN $\gamma$ 6-1mh showed the sustained treatment efficacy in the Hunner-type interstitial cystitis-like URO-OVA cystitis model**

In a subsequent experiment, the sustained effect of intravesical mIFN $\gamma$ 6-1mh was observed in the HIC-like URO-OVA cystitis model (Figure S5A). The HIC-like bladder inflammation was induced in URO-OVA mice as previously described.<sup>32</sup> The cystitis-induced mice were

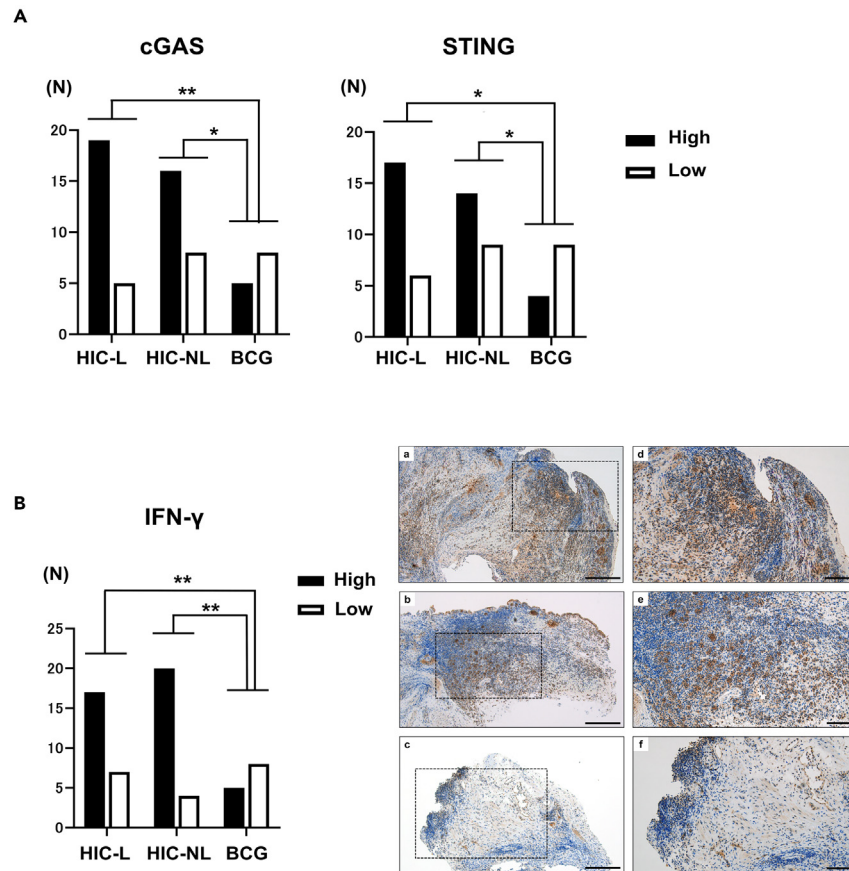


**Figure 5. Bladder immunohistochemical quantification demonstrates increased protein levels of IFN- $\gamma$ , cGAS and STING in HIC**

The immunoreactive intensities of IFN- $\gamma$ , cGAS and STING were evaluated based on the cellular (and stromal in IFN- $\gamma$ ) immunoreactive intensity as follows: negative, mild, moderate, and strong. Specimens with a negative or mild intensity were defined as having low immunoreactivity, and those with a moderate or strong intensity were defined as having high immunoreactivity.

(A) Higher immunoreactive intensities of cGAS and STING in both the Hunner lesion area (HIC-L) and non-Hunner lesion area (HIC-NL) of HIC compared to those in BCG cystitis.

(B) Higher immunoreactive intensity of IFN- $\gamma$  in both the Hunner lesion area (a, d) and non-Hunner lesion area (b, e) of HIC, compared to that in BCG cystitis (c, f) with representative immunohistochemical images. (scale bar: 250  $\mu$ m).

(d-f) Enlarged images of the areas indicated by the rectangular boxes in a-c, respectively. (scale bar: 100  $\mu$ m).

\* $p < 0.05$  and \*\* $p < 0.01$ , statistically significant by Fisher's exact test.

then intravesically treated with PBS (100  $\mu$ L,  $n = 6$ ) or mIFN $\gamma$ 6-1mh (10 nmol in 100  $\mu$ L PBS,  $n = 6$ ) on days 1, 4 and 7 after cystitis induction. To exclude the possibility that the intravesical procedure might cause bladder inflammation, sex- and age-matched cystitis-uninduced URO-OVA mice were intravesically treated with PBS (100  $\mu$ L,  $n = 6$ ) accordingly. All mice were then left without treatment till the end of the

**Table 2. The levels of mIFN $\gamma$ 6-1mh in the bladder and plasma after intravesical instillation**

Test groups <sup>a</sup>	Mouse IFN- $\gamma$ aptamer (mIFN $\gamma$ 6-1mh)	
	Amount in whole bladder (pmol/bladder)	Concentration in plasma (nM)
mIFN $\gamma$ 6-1mh (10 min)	1.821 $\pm$ 0.393 [1.83–2.50] <sup>b</sup>	7.546 $\pm$ 3.567 [0.72–12.9]
mIFN $\gamma$ 6-1mh (3 h)	0.011 $\pm$ 0.005 [0.007–0.020]	0.028 $\pm$ 0.019 [0.008–0.065]
mIFN $\gamma$ 6-1mh (24 h)	0.005 $\pm$ 0.002 [0.0016–0.0098]	0.0004 <sup>c</sup>

<sup>a</sup>Each group contains 3 samples each for the bladder and plasma.

<sup>b</sup>Mean  $\pm$  SE [range].

<sup>c</sup>Detected in 1 of 3 samples ( $n = 3$ ).

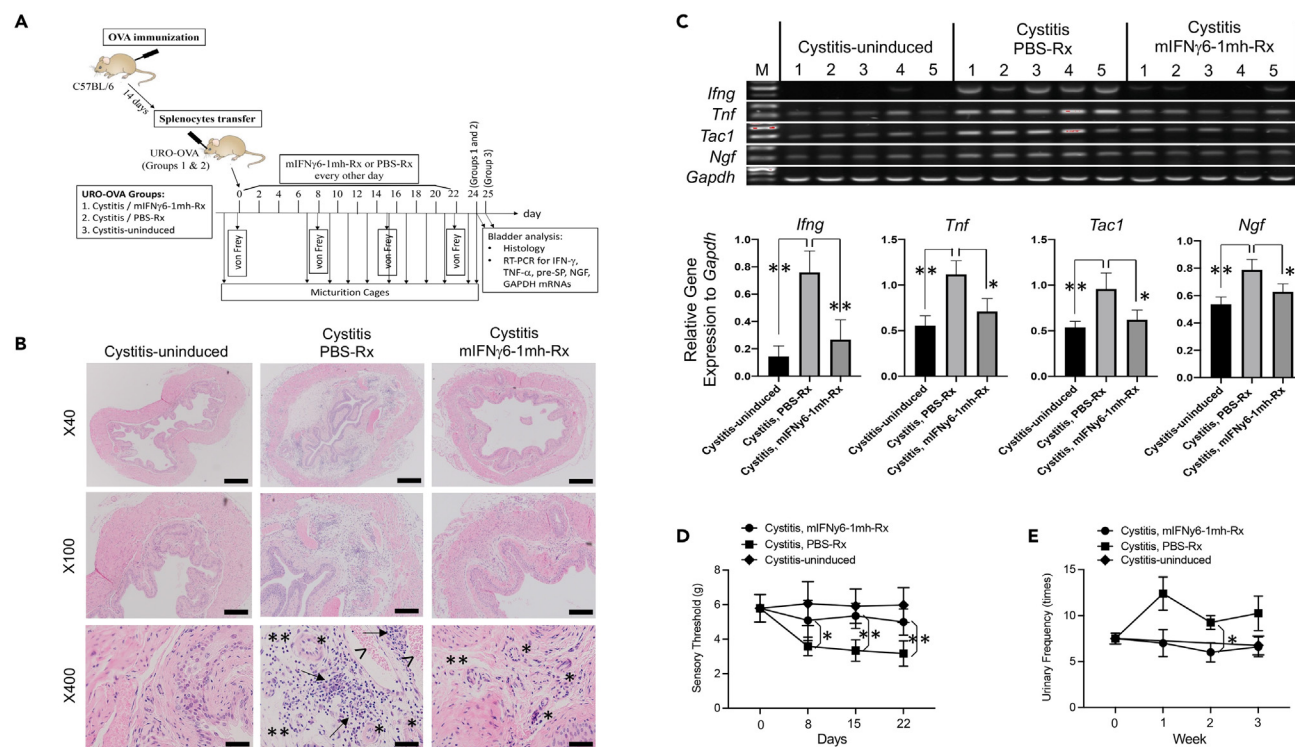


**Figure 6. Intravesical instillation of mIFN $\gamma$ 6-1mh significantly reduced bladder inflammation, pelvic nociceptive response, and urinary frequency in the HIC-like URO-OVA cystitis model**

(A) Experimental outline.

(B) Representative bladder histological images. PBS-treated cystitis mice (n = 5) showed dense mononuclear cell infiltration (arrows), increased vascularity (asterisks), mucosal hyperemia (arrowheads), and interstitial edema (horizontal double asterisks). No or mild changes were observed in cystitis-uninduced (n = 5) and mIFN $\gamma$ 6-1mh-treated cystitis mice (n = 7). Magnification: 40 $\times$  (scale bar: 500  $\mu$ m), 100 $\times$  (scale bar: 200  $\mu$ m) and 400 $\times$  (scale bar: 50  $\mu$ m).

(C) RT-PCR analysis of bladder *Ifng*, *Tnf*, *Tac1* and *Ngf* mRNAs. Top panel: Electrophoresis images of RT-PCR products from 5 bladders for each of the three groups. GAPDH was used as an internal control. M. A 100-bp DNA ladder. The image was cropped from five different gels run and exposed under the same conditions. Bottom panel: RT-PCR bands were quantified by densitometry and normalized to *Gapdh*. Data shown are the mean  $\pm$  SD relative gene expressions. \*p < 0.01 and \*\*p < 0.001.

(D) Changes in pelvic nociceptive responses during treatment. The data shown are the mean  $\pm$  SD sensory threshold for 8 baseline mice, 7 mIFN $\gamma$ 6-1mh-treated cystitis mice, 5 PBS-treated cystitis mice and 5 cystitis-uninduced mice. \*p < 0.05 and \*\*p < 0.01.

(E) Changes in urinary frequency during treatment. The data shown are the mean  $\pm$  SE urinary frequency for 8 baseline mice and 4–5 mIFN $\gamma$ 6-1mh-treated cystitis mice, PBS-treated cystitis mice, and cystitis-uninduced mice. \*p < 0.05.

See also [Figures S4](#) and [S5](#).

experiment (day 21). Bladder histological analysis showed remarkable bladder inflammation in five of the six PBS-treated cystitis mice compared with the cystitis-uninduced/PBS-treated mice ([Figure S5B](#)). Conversely, only two of the six mIFN $\gamma$ 6-1mh-treated cystitis mice exhibited similar bladder inflammation. All six cystitis-uninduced/PBS-treated mice showed no obvious bladder inflammation. Along with the histological changes, the bladders from PBS-treated cystitis mice exhibited significantly increased mRNA levels of *Ifng*, *Tnf*, *Tac1* and *Ngf*

**Table 3. Summary of the effect of intravesical mIFN $\gamma$ 6-1mh on bladder inflammation**

	Bladder Inflammatory Score			
	Grade 0	Grade 1	Grade 2	Grade 3
Cystitis-uninduced (n = 5)	3	2		
Cystitis/PBS-Rx (n = 5)		2	1	2
Cystitis/mIFN $\gamma$ 6-1mh-Rx (n = 7)	2	5		

Bladder inflammation was scored based on the degrees of inflammatory cell infiltration and stromal inflammatory changes, such as edema and vascularity. Grade 0: none or minimal inflammatory cell infiltration with few stromal changes; Grade 1: mild infiltration with mild stromal changes; Grade 2: moderate infiltration with moderate stromal changes; and Grade 3: moderate to severe infiltration with severe stromal changes.

compared with the bladders from cystitis-uninduced/PBS-treated mice (Figure S5C,  $p < 0.01$  for *Irfng*, *Tnf* and *Tac1*;  $p < 0.05$  for *Ngf*), while the bladders from mIFN $\gamma$ 6-1mh-treated cystitis mice exhibited a significantly reduced *Irfng* mRNA level ( $p < 0.01$ ) and a trend of reduction in mRNA levels of three other molecules compared with the bladders from PBS-treated cystitis mice. In addition to bladder inflammation, intravesical instillation of mIFN $\gamma$ 6-1mh significantly reversed the decreased sensory threshold for pelvic nociception compared with the intravesical instillation of PBS in cystitis mice ( $p < 0.05$  on day 8 and  $p < 0.01$  on days 14 and 21) (Figure S5D). Similarly, intravesical instillation of mIFN $\gamma$ 6-1mh completely reversed increased urinary frequency (at weeks 1 and 2) seen in the PBS-treated cystitis mice, although there was no statistical significance (Figure S5E). Our results indicated the sustained treatment effect of intravesical mIFN $\gamma$ 6-1mh in a validated HIC-like cystitis murine model, supporting the potential utility of the anti-IFN- $\gamma$  aptamer strategy for the treatment of human HIC.

## DISCUSSION

In the present study, we found Th1/17 polarized immune responses featured by prominent overexpression of IFN- $\gamma$ , enhanced cGAS-STING cytosolic DNA sensing pathway, and increased subepithelial plasma cell infiltration in the bladders of patients with HIC. We also developed an anti-mouse IFN- $\gamma$  DNA aptamer and demonstrated that the intravesical instillation of the aptamer significantly ameliorated the bladder inflammation, pelvic nociception and voiding dysfunction in an experimental murine model of HIC.

Generated evidence suggests that the skewing of immune responses toward the Th1/17 axis is responsible for the development and progression of inflammatory and autoimmune diseases, in which the major proinflammatory cytokines IFN- $\gamma$  and IL-17 coordinately play important roles.<sup>34,35</sup> Predominance of Th1 and/or Th17 immune responses has been implicated in Sjogren's syndrome (SS),<sup>34</sup> systemic lupus erythematosus (SLE),<sup>36</sup> psoriasis,<sup>37</sup> multiple sclerosis (MS),<sup>38</sup> inflammatory bowel disease (IBD),<sup>39</sup> rheumatoid arthritis (RA),<sup>40</sup> and type 1 diabetes.<sup>41</sup> Classic Th1 cells express TBX21 and IFN- $\gamma$ , whereas classic Th17 cells express RORC and IL-17. Th17 cells are known to be highly autopathogenic and can cooperate with Th1 cells to induce and promote tissue inflammation and autoimmune diseases.<sup>35</sup> In this study, we observed upregulated expression of the signature genes of Th 1/17 cells, i.e., *TBX21* and *IFN- $\gamma$*  for Th1 cells and *RORC* and *IL-17A* for Th17 cells, as well as *IL-22*, *IL-23* receptor and *TNF* produced by the Th1- and/or Th17-cell lineages in the HIC bladder (Figure 2). We also observed an increased density of IL-17A-positive cells but not total CD4-positive cells, including FOXP3-positive cells, in the HIC bladder (Figure 3). In addition, the biological pathways involved in Th1-/Th17-mediated immune responses were significantly enriched in the HIC bladder (Table S7). These observations indicate the inflammatory nature of HIC that is characterized by Th1/17 polarization.

In the present study, we observed the overexpression of cGAS and STING at both mRNA and protein levels in the HIC bladder. Our observation indicates the presence of enhanced cGAS-STING cytosolic DNA sensing pathway in the human disease. cGAS is a cytosolic DNA sensor that activates the innate immune system through the production of the second messenger cGAMP and subsequent activation of the adaptor protein STING, leading to the induction of IFNs and other inflammatory cytokines, such as TNF, IL-1 $\beta$  and IL-6.<sup>42</sup> Indeed, we observed upregulated gene expression of the major downstream products of the cGAS-STING pathway, type-1 IFN and TNF, in the HIC bladder (Figure 2A). This observation indicates the accumulation of pathogenic DNA in the cytoplasm of the HIC bladder tissues. Given the evidence that biological processes involved in infection and autoimmune responses are implicated in the pathophysiology of HIC,<sup>5,43,44</sup> the accumulated DNA could be derived from exogenous microorganisms or endogenous nuclear/mitochondrial DNA released by damaged or dead cells insulted during the infection or autoinflammation, which then led to the hyperactivation of the cGAS-STING pathway and subsequent perpetuating inflammatory reactions. Notably, it has been reported that the aberrant activation of the cGAS-STING pathway is associated with autoimmune and chronic inflammatory diseases including SS, SLE and RA,<sup>42,45</sup> the potential comorbid and associated conditions of IC/BPS.<sup>44</sup> Our observation suggests the possible involvement of the cGAS-STING pathway in HIC inflammation. In addition to cGAS and STING, we observed upregulated TLR7 gene expression in the HIC bladder (Tables S2 and S3). This observation supports our previously identified overexpression of TLR7 protein, a cytoplasm single-stranded RNA sensor, in the HIC bladder. The TLR7-related biological processes have been associated with viral infection and several autoimmune and chronic inflammatory diseases such as SS, SLE and scleroderma.<sup>46,47</sup> Microbial infection has been implicated in driving the onset of autoimmune diseases.<sup>48</sup> A recent study reported the potential association of Epstein-Barr virus infection with HIC inflammation.<sup>43</sup> Taken together, our observations highlight the importance of the nucleotide-sensing molecules potentially associated with urinary tract infection and/or autoimmune responses in HIC inflammation. Future studies are warranted to determine the origin of the accumulated intracellular pathogenic nucleic acids and the dysregulation that triggers the activation of the cGAS-STING and TLR7 pathways.

Increased plasma cell infiltration is another important histological feature of HIC. Previously, we observed increased plasma cell accumulation frequently accompanied by B-cell clonal expansion and CXCR3 overexpression in the HIC bladder.<sup>6,8</sup> This B-cell abnormality has been also implicated in other autoimmune diseases,<sup>49</sup> such as SS,<sup>50</sup> RA,<sup>51</sup> MS,<sup>52</sup> and IgG4-related cholangitis.<sup>53</sup> In the present study, this plasma cell-rich inflammatory cell infiltration, in conjunction with the upregulated biological pathways associated with CXCR3 signaling and B cell signaling/differentiation, remained robustly significant in the HIC bladder compared with the BCG cystitis bladder. Our observations support that B-cell abnormality may be another important pathological mechanism underlying HIC. Future studies that clarify the biological link between Th1/17 polarized immune responses, enhanced cytosolic nucleic acid sensing pathways, and B-cell abnormality may shed light on the pathogenesis of HIC.

In the context of our findings, it is of interest that the HIC bladder manifests gene expression patterns similar to autoimmune diseases and that patients with HIC have a high incidence of autoimmunity and high titers of autoantibodies in the serum and bladder.<sup>54,55</sup> It has been known that systemic autoimmune diseases including SS and SLE are frequently accompanied by irritative bladder disorders presenting HIC-similar symptoms.<sup>56</sup> Conversely, patients with HIC show an increased prevalence of comorbid systemic autoimmune disorders.<sup>57,58</sup>

Furthermore, female preponderance, a typical epidemiological feature of systemic autoimmune disorders, is also a well-known feature of patients with HIC.<sup>44,59</sup> In line with these observations, we observed that biological pathways related to systemic autoimmune diseases, including IBD, SLE, RA, autoimmune thyroid disease, and type 1 diabetes mellitus, were enriched in the HIC bladder (Table S7). Recently, we have conducted a genome-wide association study of patients with HIC, and identified risk loci within the major histocompatibility complex (MHC) region for HIC. The association is fine mapped to amino acid variants of class II human leukocyte antigen (HLA) genes located at the peptide binding groove, suggesting that altered antigen presentation may underlie the HIC pathogenesis.<sup>60</sup> Taken together, our observations strongly support that HIC is an immunological inflammatory disease with a possible autoimmune nature characterized by Th1/17 polarization, enhanced cGAS-STING pathway, and B-cell abnormality.

In this study, we observed prominent overexpression of IFN- $\gamma$  among various inflammatory mediators previously implicated in HIC. IFN- $\gamma$  is an important proinflammatory factor and plays a cardinal role in immune responses. In inflammatory and autoimmune diseases, IFN- $\gamma$  can contribute to systemic autoimmune responses and disease severity through its ability to promote T cell differentiation, B-cell IgG class switching, and IgG Fc receptor activation.<sup>61</sup> Aberrant IFN- $\gamma$  expression has been reported in SLE, SS, systemic sclerosis and dermatomyositis.<sup>62</sup> Studies on murine models of SLE and SS strongly support the importance of IFN- $\gamma$  in the development and progression of the human diseases.<sup>63,64</sup> Increased IFN- $\gamma$  levels were found at the peak of autoimmune inflammation at tissue-specific sites in the animal models. Interestingly, it has been demonstrated that other IFNs such as type-1 IFN (IFN- $\alpha$  and IFN- $\beta$ ) are not required for the development of autoimmune responses.<sup>65</sup> Rather, the elimination of type-1 IFN signaling exacerbated autoimmune inflammation and disease severity,<sup>66</sup> and treatment with anti-IFN- $\alpha$ R antibodies showed a minimal effect in a mouse model of SLE.<sup>67</sup>

It has been reported that treatment with an anti-IFN- $\gamma$  monoclonal antibody (mAb), soluble IFN- $\gamma$ R or cDNA encoding IFN- $\gamma$ R could reduce the serum levels of IFN- $\gamma$  and autoimmune manifestations in the animal models of SLE and SS.<sup>64,68–70</sup> However, up to date, little has been done in the development of anti-IFN- $\gamma$  antibody therapies for human diseases, except one launched for the treatment of hemophagocytic lymphohistocytosis largely due to the concerns that systemic blockade of IFN- $\gamma$  may impact both innate and adaptive immunity and be associated with severe infection. Moreover, protein-based antibodies have several intrinsic limitations. They are difficult and expensive to produce at a good manufacturing practice (GMP) scale, have relatively low stability at room temperature, and generally require systemic administration to exert pharmacological activities. To cope with these limitations, we sought to target IFN- $\gamma$  not systemically but bladder-locally with a nucleic acid aptamer, which has higher structural stability at room temperature, smaller molecular size, no immunogenicity, and rapid renal clearance compared to the conventional protein-based antibodies.

Nucleic acid aptamers are single-stranded nucleic acid molecules that can form 3D structures capable of specifically binding to various molecular targets, including proteins and cellular components.<sup>25</sup> Recently, we have generated a anti-human IFN- $\gamma$  DNA aptamer (TAGX-0003) using the SELEX method,<sup>71,72</sup> which contains our proprietary artificial nucleotide with the hydrophobic base 7-(2-thienyl)imidazo[4,5-*b*]pyridine (Ds) and demonstrates excellent affinity and specificity for human IFN- $\gamma$ . Here, to acquire animal proof-of-concept evidence that the intravesical instillation of the anti-IFN- $\gamma$  aptamer may offer a novel treatment strategy for HIC, we generated mIFN $\gamma$ 6-1mh using the same process (SELEX) and same artificial nucleotide Ds used to generate TAGX-0003. We evaluated its efficacy in our recently developed murine model of HIC, which closely reproduces clinicopathological correlates of human HIC.<sup>32</sup> Our results indicated that the intravesical instillation of mIFN $\gamma$ 6-1mh effectively ameliorated bladder inflammation, pelvic nociception, and voiding dysfunction in the HIC murine model. In addition, the serum concentration of the migrated aptamer at two days after a series of repeated instillations was very low; hence, the concern about the systemic immunosuppressive effect of the aptamer is negligible. Taken together, our results support further evaluation of the anti-IFN- $\gamma$  aptamer strategy for the treatment of human HIC.

HIC is one of the most intractable, devastating bladder disorders that severely impacts patients' QOL and has no curative treatments at present. Hence, the development of new drugs is urgently needed for patients with HIC. Our study provides a rationale for the clinical translation of the human anti-IFN- $\gamma$  DNA aptamer to a novel, effective and safe treatment for patients with HIC.

### Limitations of the study

This study has some limitations. First, the small number of the analyzed samples in both human and animal studies may bias the results. Second, we did not validate the results of the human study using independent resources. Third, superiority of the anti-IFN- $\gamma$  aptamer intravesical treatment over the currently available intravesical therapies (e.g., steroid or DMSO) has not yet been determined. Fourth, we did not investigate microbial transcriptomes in the RNA-seq analysis. In addition, we did not examine the microbial environment of the urine and bladder samples in both human and animal studies. Thus, whether microbial infection and/or local dysbiosis may affect the bladder expression of IFN- $\gamma$  gene in human and murine cystitis has not been determined. Future studies that validate the results of the present study and assure the efficacy of intravesical anti-IFN- $\gamma$  aptamer treatment should be warranted.

### STAR★METHODS

Detailed methods are provided in the online version of this paper and include the following:

- KEY RESOURCES TABLE
- RESOURCE AVAILABILITY
  - Lead contact
  - Materials availability

- Data and code availability
- **EXPERIMENTAL MODEL AND SUBJECT DETAILS**
  - Human study participants
  - Mouse strains
- **METHOD DETAILS**
  - Human study
  - Generation of the mouse IFN- $\gamma$  DNA aptamer
  - URO-OVA mouse experiments
- **QUANTIFICATION AND STATISTICAL ANALYSIS**

## SUPPLEMENTAL INFORMATION

Supplemental information can be found online at <https://doi.org/10.1016/j.isci.2023.108262>.

## ACKNOWLEDGMENTS

We would like to thank Kei Sakuma for providing technical support for the immunohistochemistry work, Shunsuke Kobayashi for anti-mouse IFN- $\gamma$  aptamer selection, and Xiaohong Chen for providing technical support for the URO-OVA mouse experiments.

This study was financially supported by the KAKENHI Grants-in-Aid from the Japanese Society for the Promotion of Science (JSPS) [Grant number 22K16788] (to YA), a Health Labour Sciences Research Grant from the Ministry of Health, Labor, and Welfare [grant number 18060798] (to YH), the Japan Agency for Medical Research and Development (AMED) [Grant number JP22nk0101229] (to M. Hori), and the National Institute of Diabetes and Digestive and Kidney Diseases (NIDDK) [Grant number R01-DK-111396] (to YL).

## AUTHOR CONTRIBUTIONS

Conceived and designed the experiments: YA and YL. Performed the experiments: YA, KH, JM, MH, KO, KF, and YL. Analyzed the data: YA, KH, JM, and YL. Wrote the article: YA, KH, and YL. Revised the article critically: KJK, MAO, DM, HK, SI, TU, DM, HK, and YH. Final approval of the version to be published: YA and YL.

## DECLARATION OF INTERESTS

This study was financially supported by TAGCyx Biotechnologies Inc.

Received: March 20, 2023

Revised: July 3, 2023

Accepted: October 17, 2023

Published: October 21, 2023

## REFERENCES

1. Homma, Y., Akiyama, Y., Tomoe, H., Furuta, A., Ueda, T., Maeda, D., Lin, A.T., Kuo, H.C., Lee, M.H., Oh, S.J., et al. (2020). Clinical guidelines for interstitial cystitis/bladder pain syndrome. *Int. J. Urol.* **27**, 578–589. <https://doi.org/10.1111/iju.14234>.
2. Clemens, J.Q., Erickson, D.R., Varela, N.P., and Lai, H.H. (2022). Diagnosis and Treatment of Interstitial Cystitis/Bladder Pain Syndrome. *J. Urol.* **208**, 34–42. <https://doi.org/10.1097/JU.0000000000002756>.
3. Patnaik, S.S., Laganà, A.S., Vitale, S.G., Buttice, S., Noventa, M., Gizzo, S., Valenti, G., Rapisarda, A.M.C., La Rosa, V.L., Magno, C., et al. (2017). Etiology, pathophysiology and biomarkers of interstitial cystitis/painful bladder syndrome. *Arch. Gynecol. Obstet.* **295**, 1341–1359. <https://doi.org/10.1007/s00404-017-4364-2>.
4. Fall, M., Nordling, J., Cervigni, M., Dinis Oliveira, P., Fariello, J., Hanno, P., Kåbjörn-Gustafsson, C., Logadottir, Y., Meijlink, J., Mishra, N., et al. (2020). Hunner lesion disease differs in diagnosis, treatment and outcome from bladder pain syndrome: an ESSIC working group report. *Scand. J. Urol.* **54**, 91–98. <https://doi.org/10.1080/21681805.2020.1730948>.
5. Akiyama, Y., Maeda, D., Katoh, H., Morikawa, T., Niimi, A., Nomiya, A., Sato, Y., Kawai, T., Goto, A., Fujimura, T., et al. (2019). Molecular Taxonomy of Interstitial Cystitis/Bladder Pain Syndrome Based on Whole Transcriptome Profiling by Next-Generation RNA Sequencing of Bladder Mucosal Biopsies. *J. Urol.* **202**, 290–300. <https://doi.org/10.1097/JU.000000000000234>.
6. Maeda, D., Akiyama, Y., Morikawa, T., Kunita, A., Ota, Y., Katoh, H., Niimi, A., Nomiya, A., Ishikawa, S., Goto, A., et al. (2015). Hunner-Type (Classic) Interstitial Cystitis: A Distinct Inflammatory Disorder Characterized by Pancystitis, with Frequent Expansion of Clonal B-Cells and Epithelial Denudation. *PLoS One* **10**, e0143316. <https://doi.org/10.1371/journal.pone.0143316>.
7. Gamper, M., Viereck, V., Eberhard, J., Binder, J., Moll, C., Welter, J., and Moser, R. (2013). Local immune response in bladder pain syndrome/interstitial cystitis ESSIC type 3C. *Int. Urogynecol. J.* **24**, 2049–2057. <https://doi.org/10.1007/s00192-013-2112-0>.
8. Akiyama, Y., Morikawa, T., Maeda, D., Shintani, Y., Niimi, A., Nomiya, A., Nakayama, A., Igawa, Y., Fukayama, M., and Homma, Y. (2016). Increased CXCR3 Expression of Infiltrating Plasma Cells in Hunner Type Interstitial Cystitis. *Sci. Rep.* **6**, 28652. <https://doi.org/10.1038/srep28652>.
9. Ogawa, T., Homma, T., Igawa, Y., Seki, S., Ishizuka, O., Imamura, T., Akahane, S., Homma, Y., and Nishizawa, O. (2010). CXCR3 binding chemokine and TNFSF14 over expression in bladder urothelium of patients with ulcerative interstitial cystitis. *J. Urol.* **183**, 1206–1212. <https://doi.org/10.1016/j.juro.2009.11.007>.
10. Ichihara, K., Aizawa, N., Akiyama, Y., Kamei, J., Masumori, N., Andersson, K.E., Homma, Y., and Igawa, Y. (2017). Toll-like receptor 7 is overexpressed in the bladder of Hunner-type interstitial cystitis, and its activation in the mouse bladder can induce cystitis and bladder pain. *Pain* **158**, 1538–1545. <https://doi.org/10.1097/j.pain.0000000000000947>.
11. Logadottir, Y., Delbro, D., Fall, M., Gjørtsson, I., Jirholt, P., Lindholm, C., and Peeker, R. (2014). Cytokine expression in patients with bladder pain syndrome/interstitial cystitis

- ESSIC type 3C. *J. Urol.* 192, 1564–1568. <https://doi.org/10.1016/j.juro.2014.04.099>.
12. Soucy, F., and Grégoire, M. (2005). Efficacy of prednisone for severe refractory ulcerative interstitial cystitis. *J. Urol.* 173, 841–843. , discussion 843. <https://doi.org/10.1097/01.ju.0000153612.14639.19>.
  13. Forrest, J.B., Payne, C.K., and Erickson, D.R. (2012). Cyclosporine A for refractory interstitial cystitis/bladder pain syndrome: experience of 3 tertiary centers. *J. Urol.* 188, 1186–1191. <https://doi.org/10.1016/j.juro.2012.06.023>.
  14. Bosch, P.C. (2018). A Randomized, Double-blind, Placebo-controlled Trial of Certolizumab Pegol in Women with Refractory Interstitial Cystitis/Bladder Pain Syndrome. *Eur. Urol.* 74, 623–630. <https://doi.org/10.1016/j.eururo.2018.07.026>.
  15. Fall, M., Baranowski, A.P., Elneil, S., Engeler, D., Hughes, J., Messelink, E.J., Oberpenning, F., and de C Williams, A.C.; European Association of Urology (2010). EAU guidelines on chronic pelvic pain. *Eur. Urol.* 57, 35–48. <https://doi.org/10.1016/j.eururo.2009.08.020>.
  16. Funaro, M.G., King, A.N., Stern, J.N.H., Moldwin, R.M., and Bahlani, S. (2018). Endoscopic Injection of Low Dose Triamcinolone: A Simple, Minimally Invasive, and Effective Therapy for Interstitial Cystitis With Hunner Lesions. *Urology* 118, 25–29. <https://doi.org/10.1016/j.urology.2018.03.037>.
  17. Yoshimura, N., Homma, Y., Tomoe, H., Otsuka, A., Kitta, T., Masumori, N., Akiyama, Y., Niimi, A., Mitsui, T., Nanri, M., et al. (2021). Efficacy and safety of intravesical instillation of KRP-116D (50% dimethyl sulfoxide solution) for interstitial cystitis/bladder pain syndrome in Japanese patients: A multicenter, randomized, double-blind, placebo-controlled, clinical study. *Int. J. Urol.* 28, 545–553. <https://doi.org/10.1111/iju.14505>.
  18. Niimi, A., Igawa, Y., Aizawa, N., Honma, T., Nomiya, A., Akiyama, Y., Kamei, J., Fujimura, T., Fukuhara, H., and Homma, Y. (2018). Diagnostic value of urinary CXCL10 as a biomarker for predicting Hunner type interstitial cystitis. *Neurourol. Urodyn.* 37, 1113–1119. <https://doi.org/10.1002/nau.23431>.
  19. Furuta, A., Yamamoto, T., Suzuki, Y., Gotoh, M., Egawa, S., and Yoshimura, N. (2018). Comparison of inflammatory urine markers in patients with interstitial cystitis and overactive bladder. *Int. Urogynecol. J.* 29, 961–966. <https://doi.org/10.1007/s00192-017-3547-5>.
  20. Akiyama, Y., Miyakawa, J., O'Donnell, M.A., Kreder, K.J., Luo, Y., Maeda, D., Ushiku, T., Kume, H., and Homma, Y. (2022). Overexpression of HIF1alpha in Hunner Lesions of Interstitial Cystitis: Pathophysiological Implications. *J. Urol.* 207, 635–646. <https://doi.org/10.1097/JU.0000000000002278>.
  21. Lopez-Beltran, A., Luque, R.J., Mazzucchelli, R., Scarpelli, M., and Montironi, R. (2002). Changes produced in the urothelium by traditional and newer therapeutic procedures for bladder cancer. *J. Clin. Pathol.* 55, 641–647. <https://doi.org/10.1136/jcp.55.9.641>.
  22. El-Zaatar, Z.M., and Ro, J.Y. (2021). Normal Anatomy and Histology of the Urinary Bladder with Pathologic Correlates. In *Urinary Bladder Pathology* (Springer), pp. 7–20.
  23. Poletajew, S., Krajewski, W., Adamowicz, J., and Radziszewski, P. (2019). A systematic review of preventive and therapeutic options for symptoms of cystitis in patients with bladder cancer receiving intravesical bacillus Calmette-Guerin immunotherapy. *Anti Cancer Drugs* 30, 517–522. <https://doi.org/10.1097/CAD.0000000000000775>.
  24. Ritz, N., Dutta, B., Donath, S., Casalaz, D., Connell, T.G., Tebruegge, M., Robins-Browne, R., Hanekom, W.A., Britton, W.J., and Curtis, N. (2012). The influence of bacille Calmette-Guerin vaccine strain on the immune response against tuberculosis: a randomized trial. *Am. J. Respir. Crit. Care Med.* 185, 213–222. <https://doi.org/10.1164/rccm.201104-0714OC>.
  25. Keefe, A.D., Pai, S., and Ellington, A. (2010). Aptamers as therapeutics. *Nat. Rev. Drug Discov.* 9, 537–550. <https://doi.org/10.1038/nrd3141>.
  26. van de Merwe, J.P., Nordling, J., Bouchelouche, P., Bouchelouche, K., Cervigni, M., Daha, L.K., Elneil, S., Fall, M., Hohlbrugger, G., Irwin, P., et al. (2008). Diagnostic criteria, classification, and nomenclature for painful bladder syndrome/interstitial cystitis: an ESSIC proposal. *Eur. Urol.* 53, 60–67. <https://doi.org/10.1016/j.eururo.2007.09.019>.
  27. Babjuk, M., Burger, M., Capoun, O., Cohen, D., Compérat, E.M., Dominguez Escrig, J.L., Gontero, P., Liedberg, F., Masson-Lecomte, A., Mostafid, A.H., et al. (2022). European Association of Urology Guidelines on Non-muscle-invasive Bladder Cancer (Ta, T1, and Carcinoma in Situ). *Eur. Urol.* 81, 75–94. <https://doi.org/10.1016/j.eururo.2021.08.010>.
  28. O'Leary, M.P., Sant, G.R., Fowler, F.J., Jr., Whitmore, K.E., and Spolarich-Kroll, J. (1997). The interstitial cystitis symptom index and problem index. *Urology* 49, 58–63. [https://doi.org/10.1016/s0090-4295\(99\)80333-1](https://doi.org/10.1016/s0090-4295(99)80333-1).
  29. Akiyama, Y., Maeda, D., Morikawa, T., Niimi, A., Nomiya, A., Yamada, Y., Igawa, Y., Goto, A., Fukayama, M., and Homma, Y. (2018). Digital quantitative analysis of mast cell infiltration in interstitial cystitis. *Neurourol. Urodyn.* 37, 650–657. <https://doi.org/10.1002/nau.23365>.
  30. Song, S., Peng, P., Tang, Z., Zhao, J., Wu, W., Li, H., Shao, M., Li, L., Yang, C., Duan, F., et al. (2017). Decreased expression of STING predicts poor prognosis in patients with gastric cancer. *Sci. Rep.* 7, 39858. <https://doi.org/10.1038/srep39858>.
  31. Kimoto, M., Matsunaga, K.I., and Hirao, I. (2017). Evolving Aptamers with Unnatural Base Pairs. *Curr. Protoc. Chem. Biol.* 9, 315–339. <https://doi.org/10.1002/cpcb.31>.
  32. Akiyama, Y., Yao, J.R., Kreder, K.J., O'Donnell, M.A., Lutgendorf, S.K., Lyu, D., Maeda, D., Kume, H., Homma, Y., and Luo, Y. (2021). Autoimmunity to urothelial antigen causes bladder inflammation, pelvic pain, and voiding dysfunction: a novel animal model for Hunner-type interstitial cystitis. *Am. J. Physiol. Ren. Physiol.* 320, F174–F182. <https://doi.org/10.1152/ajprenal.00290.2020>.
  33. Liu, W., Evanoff, D.P., Chen, X., and Luo, Y. (2007). Urinary bladder epithelium antigen induces CD8+ T cell tolerance, activation, and autoimmune response. *J. Immunol.* 178, 539–546. <https://doi.org/10.4049/jimmunol.178.1.539>.
  34. Katsifis, G.E., Rekka, S., Moutsopoulos, N.M., Pillemer, S., and Wahl, S.M. (2009). Systemic and local interleukin-17 and linked cytokines associated with Sjogren's syndrome immunopathogenesis. *Am. J. Pathol.* 175, 1167–1177. <https://doi.org/10.2353/ajpath.2009.090319>.
  35. Afzali, B., Lombardi, G., Lechler, R.I., and Lord, G.M. (2007). The role of T helper 17 (Th17) and regulatory T cells (Treg) in human organ transplantation and autoimmune disease. *Clin. Exp. Immunol.* 148, 32–46. <https://doi.org/10.1111/j.1365-2249.2007.03356.x>.
  36. Wong, C.K., Ho, C.Y., Li, E.K., and Lam, C.W. (2000). Elevation of proinflammatory cytokine (IL-18, IL-17, IL-12) and Th2 cytokine (IL-4) concentrations in patients with systemic lupus erythematosus. *Lupus* 9, 589–593. <https://doi.org/10.1191/096120300678828703>.
  37. Arican, O., Aral, M., Sasmaz, S., and Ciragil, P. (2005). Serum levels of TNF-alpha, IFN-gamma, IL-6, IL-8, IL-12, IL-17, and IL-18 in patients with active psoriasis and correlation with disease severity. *Mediat. Inflamm.* 2005, 273–279. <https://doi.org/10.1155/MI.2005.273>.
  38. Matusevicius, D., Kivisäkk, P., He, B., Kostulas, N., Ozenci, V., Fredrikson, S., and Link, H. (1999). Interleukin-17 mRNA expression in blood and CSF mononuclear cells is augmented in multiple sclerosis. *Mult. Scler.* 5, 101–104. <https://doi.org/10.1177/135245859900500206>.
  39. Fujino, S., Andoh, A., Bamba, S., Ogawa, A., Hata, K., Araki, Y., Bamba, T., and Fujiyama, Y. (2003). Increased expression of interleukin 17 in inflammatory bowel disease. *Gut* 52, 65–70. <https://doi.org/10.1136/gut.52.1.65>.
  40. Miossec, P. (2003). Interleukin-17 in rheumatoid arthritis: if T cells were to contribute to inflammation and destruction through synergy. *Arthritis Rheum.* 48, 594–601. <https://doi.org/10.1002/art.10816>.
  41. Bradshaw, E.M., Raddassi, K., Elyaman, W., Orban, T., Gottlieb, P.A., Kent, S.C., and Hafler, D.A. (2009). Monocytes from patients with type 1 diabetes spontaneously secrete proinflammatory cytokines inducing Th17 cells. *J. Immunol.* 183, 4432–4439. <https://doi.org/10.4049/jimmunol.0900576>.
  42. Chen, Q., Sun, L., and Chen, Z.J. (2016). Regulation and function of the cGAS-STING pathway of cytosolic DNA sensing. *Nat. Immunol.* 17, 1142–1149. <https://doi.org/10.1038/ni.3558>.
  43. Jhang, J.F., Liu, C.D., Hsu, Y.H., Chen, C.C., Chen, H.C., Jiang, Y.H., Wu, W.C., Peng, C.W., and Kuo, H.C. (2023). EBV infection mediated BDNF expression is associated with bladder inflammation in interstitial cystitis/bladder pain syndrome with Hunner's lesion. *J. Pathol.* 259, 276–290. <https://doi.org/10.1002/path.6040>.
  44. van de Merwe, J.P. (2007). Interstitial cystitis and systemic autoimmune diseases. *Nat. Clin. Pract. Urol.* 4, 484–491. <https://doi.org/10.1038/ncpuro0874>.
  45. Decout, A., Katz, J.D., Venkatraman, S., and Ablasser, A. (2021). The cGAS-STING pathway as a therapeutic target in inflammatory diseases. *Nat. Rev. Immunol.* 21, 548–569. <https://doi.org/10.1038/s41577-021-00524-z>.
  46. Marshak-Rothstein, A. (2006). Toll-like receptors in systemic autoimmune disease. *Nat. Rev. Immunol.* 6, 823–835. <https://doi.org/10.1038/nri1957>.
  47. Duffy, L., and O'Reilly, S.C. (2016). Toll-like receptors in the pathogenesis of autoimmune diseases: recent and emerging translational developments. *ImmunoTargets*

- Ther. 5, 69–80. <https://doi.org/10.2147/ITT.589795>.
48. Floreani, A., Leung, P.S.C., and Gershwin, M.E. (2016). Environmental Basis of Autoimmunity. *Clin. Rev. Allergy Immunol.* 50, 287–300. <https://doi.org/10.1007/s12016-015-8493-8>.
  49. Ferraccioli, G., and Tulusso, B. (2007). Infections, B cell receptor activation and autoimmunity: different check-point impairments lead to autoimmunity, clonal B cell expansion and fibrosis in different immunological settings. *Autoimmun. Rev.* 7, 109–113. <https://doi.org/10.1016/j.autrev.2007.02.013>.
  50. Bahler, D.W., and Swerdlow, S.H. (1998). Clonal salivary gland infiltrates associated with myoepithelial sialadenitis (Sjogren's syndrome) begin as nonmalignant antigen-selected expansions. *Blood* 91, 1864–1872.
  51. Doorenspleet, M.E., Klarenbeek, P.L., de Hair, M.J.H., van Schaik, B.D.C., Esveldt, R.E.E., van Kampen, A.H.C., Gerlag, D.M., Musters, A., Baas, F., Tak, P.P., and de Vries, N. (2014). Rheumatoid arthritis synovial tissue harbours dominant B-cell and plasma-cell clones associated with autoreactivity. *Ann. Rheum. Dis.* 73, 756–762. <https://doi.org/10.1136/annrheumdis-2012-202861>.
  52. Owens, G.P., Ritchie, A.M., Burgoon, M.P., Williamson, R.A., Corboy, J.R., and Gilden, D.H. (2003). Single-cell repertoire analysis demonstrates that clonal expansion is a prominent feature of the B cell response in multiple sclerosis cerebrospinal fluid. *J. Immunol.* 171, 2725–2733. <https://doi.org/10.4049/jimmunol.171.5.2725>.
  53. Maillette de Buy Wenniger, L.J., Doorenspleet, M.E., Klarenbeek, P.L., Verheij, J., Baas, F., Elferink, R.P.O., Tak, P.P., de Vries, N., and Beuers, U. (2013). Immunoglobulin G4+ clones identified by next-generation sequencing dominate the B cell receptor repertoire in immunoglobulin G4 associated cholangitis. *Hepatology* 57, 2390–2398. <https://doi.org/10.1002/hep.26232>.
  54. Jokinen, E.J., Alftan, O.S., and Oravisto, K.J. (1972). Antitissue antibodies in interstitial cystitis. *Clin. Exp. Immunol.* 11, 333–339.
  55. Ochs, R.L., Stein, T.W., Jr., Peebles, C.L., Gittes, R.F., and Tan, E.M. (1994). Autoantibodies in interstitial cystitis. *J. Urol.* 151, 587–592. [https://doi.org/10.1016/s0022-5347\(17\)35023-1](https://doi.org/10.1016/s0022-5347(17)35023-1).
  56. Haarala, M., Alanen, A., Hietarinta, M., and Kiilholma, P. (2000). Lower urinary tract symptoms in patients with Sjogren's syndrome and systemic lupus erythematosus. *Int. UrogynEcol. J. Pelvic Floor Dysfunct.* 11, 84–86.
  57. Peeker, R., Atanasiu, L., and Logadottir, Y. (2003). Intercurrent autoimmune conditions in classic and non-ulcer interstitial cystitis. *Scand. J. Urol. Nephrol.* 37, 60–63. <https://doi.org/10.1080/00365590310008721>.
  58. Yueh, H.Z., Yang, M.H., Huang, J.Y., and Wei, J.C.C. (2021). Risk of Autoimmune Diseases in Patients With Interstitial Cystitis/Bladder Pain Syndrome: A Nationwide Population-Based Study in Taiwan. *Front. Med.* 8, 747098. <https://doi.org/10.3389/fmed.2021.747098>.
  59. Probert, K.J., Schaeffer, A.J., Brensinger, C.M., Kusek, J.W., Nyberg, L.M., and Landis, J.R. (2000). A prospective study of interstitial cystitis: results of longitudinal followup of the interstitial cystitis data base cohort. The Interstitial Cystitis Data Base Study Group. *J. Urol.* 163, 1434–1439. [https://doi.org/10.1016/s0022-5347\(05\)67637-9](https://doi.org/10.1016/s0022-5347(05)67637-9).
  60. Akiyama, Y., Sonehara, K., Maeda, D., Katoh, H., Naito, T., Yamamoto, K., Biobank Japan Project, Morisaki, T., Ishikawa, S., Ushiku, T., et al. (2023). Genome-wide association study identifies risk loci within the major histocompatibility complex region for Hunner-type interstitial cystitis. *Cell Rep. Med.* 4, 101114. <https://doi.org/10.1016/j.xcrm.2023.101114>.
  61. Baudino, L., Azeredo da Silveira, S., Nakata, M., and Izui, S. (2006). Molecular and cellular basis for pathogenicity of autoantibodies: lessons from murine monoclonal autoantibodies. *Springer Semin. Immunopathol.* 28, 175–184. <https://doi.org/10.1007/s00281-006-0037-0>.
  62. Pollard, K.M., Cauvi, D.M., Toomey, C.B., Morris, K.V., and Kono, D.H. (2013). Interferon-gamma and systemic autoimmunity. *Discov. Med.* 16, 123–131.
  63. Enghard, P., Langnickel, D., and Riemekasten, G. (2006). T cell cytokine imbalance towards production of IFN-gamma and IL-10 in NZB/W F1 lupus-prone mice is associated with autoantibody levels and nephritis. *Scand. J. Rheumatol.* 35, 209–216. <https://doi.org/10.1080/03009740500417791>.
  64. Nguyen, C.Q., and Peck, A.B. (2013). The Interferon-Signature of Sjogren's Syndrome: How Unique Biomarkers Can Identify Underlying Inflammatory and Immunopathological Mechanisms of Specific Diseases. *Front. Immunol.* 4, 142. <https://doi.org/10.3389/fimmu.2013.00142>.
  65. Nickerson, K.M., Cullen, J.L., Kashgarian, M., and Shlomchik, M.J. (2013). Exacerbated autoimmunity in the absence of TLR9 in MRL.Fas(lpr) mice depends on Ifnar1. *J. Immunol.* 190, 3889–3894. <https://doi.org/10.4049/jimmunol.1203525>.
  66. Hron, J.D., and Peng, S.L. (2004). Type I IFN protects against murine lupus. *J. Immunol.* 173, 2134–2142. <https://doi.org/10.4049/jimmunol.173.3.2134>.
  67. Baccala, R., Gonzalez-Quintal, R., Schreiber, R.D., Lawson, B.R., Kono, D.H., and Theofilopoulos, A.N. (2012). Anti-IFN-alpha/beta receptor antibody treatment ameliorates disease in lupus-predisposed mice. *J. Immunol.* 189, 5976–5984. <https://doi.org/10.4049/jimmunol.1201477>.
  68. Jacob, C.O., van der Meide, P.H., and McDevitt, H.O. (1987). In vivo treatment of (NZB X NZW)F1 lupus-like nephritis with monoclonal antibody to gamma interferon. *J. Exp. Med.* 166, 798–803. <https://doi.org/10.1084/jem.166.3.798>.
  69. Ozmen, L., Roman, D., Fountoulakis, M., Schmid, G., Ryffel, B., and Garotta, G. (1995). Experimental therapy of systemic lupus erythematosus: the treatment of NZB/W mice with mouse soluble interferon-gamma receptor inhibits the onset of glomerulonephritis. *Eur. J. Immunol.* 25, 6–12. <https://doi.org/10.1002/eji.1830250103>.
  70. Lawson, B.R., Prud'homme, G.J., Chang, Y., Gardner, H.A., Kuan, J., Kono, D.H., and Theofilopoulos, A.N. (2000). Treatment of murine lupus with cDNA encoding IFN-gammaR/Fc. *J. Clin. Invest.* 106, 207–215. <https://doi.org/10.1172/JCI10167>.
  71. Kimoto, M., Yamashige, R., Matsunaga, K.i., Yokoyama, S., and Hirao, I. (2013). Generation of high-affinity DNA aptamers using an expanded genetic alphabet. *Nat. Biotechnol.* 31, 453–457. <https://doi.org/10.1038/nbt.2556>.
  72. Matsunaga, K.i., Kimoto, M., Hanson, C., Sanford, M., Young, H.A., and Hirao, I. (2015). Architecture of high-affinity unnatural-base DNA aptamers toward pharmaceutical applications. *Sci. Rep.* 5, 18478. <https://doi.org/10.1038/srep18478>.
  73. Dobin, A., Davis, C.A., Schlesinger, F., Drenkow, J., Zaleski, C., Jha, S., Batut, P., Chaisson, M., and Gingeras, T.R. (2013). STAR: ultrafast universal RNA-seq aligner. *Bioinformatics* 29, 15–21. <https://doi.org/10.1093/bioinformatics/bts635>.
  74. Futami, K., Kimoto, M., Lim, Y.W.S., and Hirao, I. (2019). Genetic Alphabet Expansion Provides Versatile Specificities and Activities of Unnatural-Base DNA Aptamers Targeting Cancer Cells. *Mol. Ther. Nucleic Acids* 14, 158–170. <https://doi.org/10.1016/j.omtn.2018.11.011>.
  75. Gilhar, A., Keren, A., Shemer, A., d'Ovidio, R., Ullmann, Y., and Paus, R. (2013). Autoimmune disease induction in a healthy human organ: a humanized mouse model of alopecia areata. *J. Invest. Dermatol.* 133, 844–847. <https://doi.org/10.1038/jid.2012.365>.

STAR★METHODS

KEY RESOURCES TABLE

REAGENT or RESOURCE	SOURCE	IDENTIFIER
<b>Antibodies</b>		
Mouse monoclonal anti-human CD3, clone LN10	Novocastra	clone LN1; RRID:AB_30736190
Rabbit monoclonal anti-human CD4, clone SP35	Roche	clone SP35; RRID:AB_2335982
Mouse monoclonal anti-human CD8, clone 4B11	Leica Biosystems	clone 4B11; RRID:AB_10555292
Mouse monoclonal anti-human CD20, clone L26	Dako	clone L26; RRID:AB_2282030
Mouse monoclonal anti-human CD138, clone B-A38	Nichirei Bioscience	clone B-A38; RRID:AB_1860097
Rabbit anti-human cGAS (MB21D1)	Sigma–Aldrich	HPA031700; RRID:AB_10601693
Mouse monoclonal anti-human cytokeratin, clone AE1+AE3	Dako	clone AE1+AE3; RRID:AB_2631307
Mouse monoclonal anti-human FOXP3, clone 236A/E7	Abcam	clone 236A/E7; RRID:AB_445284
Mouse monoclonal anti-human IFN- $\gamma$	Abcam	ab218890; RRID:AB_2847937
Goat anti-human IL-17A	R&D Systems	AF-317-NA; RRID:AB_354463
Mouse monoclonal anti-human mast cell tryptase (MCT), clone AA1	Dako	clone AA1; RRID:AB_2206478
Rabbit anti-human STING (TMEM173)	Sigma–Aldrich	HPA038116; RRID:AB_2675841
Alexa Fluor 488-conjugated mouse anti-STAT1 (pY701) antibody	BD Bioscience	Cat#612596; RRID:AB_399879
<b>Biological samples</b>		
Human bladder biopsy tissues	This study	N/A
Human total RNA extracted from bladder tissues	This study	N/A
URO-OVA mouse bladder tissues	This study	N/A
URO-OVA mouse total RNA extracted from bladder tissues	This study	N/A
<b>Chemicals, peptides, and recombinant proteins</b>		
Recombinant mouse IFN- $\gamma$ proteins	Sino Biological	#50709-M02H, #50709-MNAH
<b>Critical commercial assays</b>		
NucleoSpin RNA	Macherey-Nagel	Cat#740955.50
SMART-Seq v4 Ultra Low Input RNA kit	Clontech	Cat#634888
Nextera XT DNA Library Preparation Kit	Illumina	Cat#FC-131-1024
SuperScript VIL0 cDNA synthesis kit	Invitrogen	Cat#11754050
TaqMan® Universal Master Mix II, no UNG	Applied Biosystems	Cat#4440043
KOD SYBR qPCR mix kit	TOYOBO	Cat#QKD-201
QIAquick PCR purification kit	Qiagen	Cat#28104, 28106
<b>Deposited data</b>		
Gene expression Omnibus (GEO)	<a href="http://www.ncbi.nlm.nih.gov/geo/">www.ncbi.nlm.nih.gov/geo/</a>	GEO Accession #: GSE238208
<b>Experimental models: Cell lines</b>		
mouse derived L929 fibroblast cell line	RIKEN Bioresource Research Center Cell Bank	Cat#RCB1422
<b>Experimental models: Organisms/strains</b>		
Mouse: CD-1, CrI:CD1(ICR)	Jackson Laboratory	CrI:CD1(ICR)
Mouse: URO-OVA: C57BL/6 genetic background	University of Iowa	N/A
Mouse: C57BL/6	Charles River	C57BL/6NcrI

(Continued on next page)

Continued

REAGENT or RESOURCE	SOURCE	IDENTIFIER
<b>Oligonucleotides</b>		
IL2	Thermo Fisher Scientific	Cat#Hs00174114_m1
IL4	Thermo Fisher Scientific	Cat#Hs00174122_m1
IL6	Thermo Fisher Scientific	Cat#Hs00174131_m1
IL10	Thermo Fisher Scientific	Cat#Hs00961622_m1
IL12A	Thermo Fisher Scientific	Cat#Hs01073447_m1
IL12B	Thermo Fisher Scientific	Cat#Hs01011518_m1
IL17A	Thermo Fisher Scientific	Cat#Hs00174383_m1
IL22	Thermo Fisher Scientific	Cat#Hs01574154_m1
IL23R	Thermo Fisher Scientific	Cat#Hs00332759_m1
HIF1A	Thermo Fisher Scientific	Cat#Hs00153153_m1
IFNA17	Thermo Fisher Scientific	Cat#Hs00819693_sH
IFNB1	Thermo Fisher Scientific	Cat#Hs01077958_s1
IFNG	Thermo Fisher Scientific	Cat#Hs00989291_m1
TNF	Thermo Fisher Scientific	Cat#Hs00174128_m1
TGFB1	Thermo Fisher Scientific	Cat#Hs00998133_m1
TBX21 (T-bet)	Thermo Fisher Scientific	Cat#Hs00894392_m1
GATA3	Thermo Fisher Scientific	Cat#Hs00231122_m1
RORC	Thermo Fisher Scientific	Cat#Hs01076112_m1
CTLA4	Thermo Fisher Scientific	Cat#Hs00175480_m1
cGAS (MB21D1)	Thermo Fisher Scientific	Cat#Hs00403553_m1
STING (TMEM173)	Thermo Fisher Scientific	Cat#Hs00736955_g1
IPO8	Thermo Fisher Scientific	Cat#Hs00183533_m1
primer pairs for <i>Irfng</i> : 5'-TGAACGCTACACACTGCATCT-3' and 5'-GACTCCTTTCCGCTTCCTGA-3' (459 bp)	Integrated DNA Technologies	N/A
primer pairs for <i>Tnf</i> : 5'-CGTCAGCCGATTTGCTATCT-3' and 5'-CGGACTCCGCAAAGCTAAG-3' (206 bp)	Integrated DNA Technologies	N/A
primer pairs for <i>Tac1</i> : 5'-GCCAATGCAGAACTACGAAA-3' and 5'-GCTTGACAGCTCCTTCATC-3' (280 bp)	Integrated DNA Technologies	N/A
primer pairs for <i>Ngf</i> : 5'-CTGTAGACCCAGACTGTTT-3' and 5'-CACTGAGAACTCCCCATGT-3' (194 bp)	Integrated DNA Technologies	N/A
primer pairs for <i>Gapdh</i> : 5'-GTTCCAGTATGACTCCACT-3' and 5'-GTGCAGGATGCATTGCTG-3' (321 bp)	Integrated DNA Technologies	N/A
mIFN $\gamma$ 5-1mh: 5'-CCGCACCGATGACTGGTACCCATGTACAGGTCAC DsTTGGCCTCTTCGDsGTGCGGCGGAAGCG-3'	This study	N/A
mIFN $\gamma$ 6-1mh: 5'-GGCCGGTACCCGADsCCACAGTTTATDsGTTGTACT AGTTTTGCAGGGTCTGGCCCGGAAGCG-3'	This study	N/A
Negative control DNA: 5'-CGACTTTTTTATATTTTTTTGTCGCGGAAGCG-3'	This study	N/A
Primer pairs for mIFN $\gamma$ 6-1mh: 5'-GGCCGGTACCCGAACCACAGTTTATAGTTGTACTA-3' and 5'-CGCTTCGCGGGCCAGACCCTGC-3'	This study	N/A
<b>Software and algorithms</b>		
NovaSeq Control Software	Illumina	<a href="https://support.illumina.com/downloads/novaseq-control-software-v1-8.html">https://support.illumina.com/downloads/novaseq-control-software-v1-8.html</a>

(Continued on next page)

**Continued**

REAGENT or RESOURCE	SOURCE	IDENTIFIER
Illumina bclfastq 2.20	Illumina	<a href="https://support.illumina.com/downloads/bcl2fastq-conversion-software-v2-20.html">https://support.illumina.com/downloads/bcl2fastq-conversion-software-v2-20.html</a>
Genedata Profiler Genome ver. 11.0.8	Genedata	<a href="https://www.genedata.com/products-services/profiler/software">https://www.genedata.com/products-services/profiler/software</a>
STAR ver. 2.5.3a	Dobin et al. <sup>73</sup>	<a href="http://code.google.com/p/ma-star/">http://code.google.com/p/ma-star/</a>
Genedata Analyst ver. 9.1.13	Genedata	<a href="https://www.genedata.com/products-services/selector/software/analyst">https://www.genedata.com/products-services/selector/software/analyst</a>
Agilent Gene Spring software packages ver. 14.8	Agilent Technologies	<a href="https://www.agilent.com/en/product/software-informatics/genomics-software-informatics/gene-expression/genespring-gx">https://www.agilent.com/en/product/software-informatics/genomics-software-informatics/gene-expression/genespring-gx</a>
Gene Ontology/Gene Ontology Slim analyses	THE GENE ONTOLOGY RESOURCE	<a href="http://www.geneontology.org/">http://www.geneontology.org/</a>
KEGG pathway enrichment analysis	KEGG PATHWAY Database	<a href="https://www.genome.jp/kegg/pathway.html">https://www.genome.jp/kegg/pathway.html</a>
Tissue Studio ver. 3.5	Definiens	<a href="https://www.biocompare.com/19333-Image-Analysis-Software-Image-Processing-Software/4378970-Definiens-Tissue-Studio/">https://www.biocompare.com/19333-Image-Analysis-Software-Image-Processing-Software/4378970-Definiens-Tissue-Studio/</a>
Oxymax software	Columbus Instruments	<a href="https://www.colinst.com/default.aspx">https://www.colinst.com/default.aspx</a>
GraphPad Prism ver. 8	GraphPad	<a href="https://www.graphpad.com/">https://www.graphpad.com/</a>
ImageJ	USA National Institutes of Health	<a href="http://rsb.info.nih.gov/ij">http://rsb.info.nih.gov/ij</a>
De Novo software	FCS Express	<a href="https://denovosoftware.com/">https://denovosoftware.com/</a>
<b>Other</b>		
Illumina NovaSeq 6000	Illumina	<a href="https://www.illumina.com/systems/sequencing-platforms/novaseq.html">https://www.illumina.com/systems/sequencing-platforms/novaseq.html</a>
NanoZoomer Digital Pathology system	Hamamatsu Photonics	<a href="https://nanozoomer.hamamatsu.com/us/en.html">https://nanozoomer.hamamatsu.com/us/en.html</a>

**RESOURCE AVAILABILITY****Lead contact**

Further information and requests should be directed to the lead contact, Yoshiyuki Akiyama ([yoshiyuki-akiyama@uiowa.edu](mailto:yoshiyuki-akiyama@uiowa.edu)).

**Materials availability**

Further information and requests for the generated mouse anti-IFN $\gamma$  DNA aptamer (mIFN $\gamma$ -1mh) should be directed to Miyuki Hori, TAGCyx Biotechnologies Inc ([m\\_hori@tagcyx.com](mailto:m_hori@tagcyx.com)).

**Data and code availability**

RNA-sequence data of bladder mucosal biopsies of patients with HIC and BCG cystitis, including raw sequence data and processed data (FPKM values for each sample), was deposited at the Gene Expression Omnibus (<https://www.ncbi.nlm.nih.gov/geo/>) and are publicly available with the accession ID #GSE238208. This study does not contain original codes. Any additional information required to reanalyze the data reported in this work is available from the [lead contact](#) upon request.

**EXPERIMENTAL MODEL AND SUBJECT DETAILS****Human study participants**

The participants in the human study included 25 patients (23 females) diagnosed with HIC who underwent and responded to endoscopic electrocautery of Hunner lesions with bladder hydrodistension and 13 patients (5 females) who developed chronic cystitis after prophylactic or therapeutic intravesical instillation of BCG for NMIBC. They were recruited at The University of Tokyo Hospital between 2016 and 2019. Diagnosis of HIC was made according to the East Asian clinical guidelines and the ESSIC criteria by two urologists with expertise in managing IC/BPS who are both board members of the East Asian IC/BPS Clinical Guidelines Committee (YA, YH).<sup>1,26</sup> Diagnosis of BCG-related cystitis was made based on histological evidence of granulation tissue, epithelial denudation, increased neovascularization, stromal edema and fibrosis, and dense subepithelial lymphocytic infiltration with frequent formation of lymphoid follicles or aggregates, with a negative urine culture and previous history of BCG therapy.

Patient demographic information was retrieved from medical records and included the IC/BPS symptom scores measured by OSSI/OSPI index,<sup>28</sup> a most popular, validated symptom indices for IC/BPS; an 11-point numerical rating of pain intensity, with 0 indicating no pain and 10 indicating the worst pain ever; a 7-grade QOL scale derived from the International Prostate Symptom Score, with 0 indicating excellent and 6 indicating terrible; daytime and nocturnal urinary frequency; maximum and average voided volume; and bladder capacity measured at bladder hydrodistension at a pressure of 80 cm H<sub>2</sub>O under general anesthesia.

### Mouse strains

URO-OVA mice were previously developed in our laboratory and they were on the C57BL/6 genetic background.<sup>33</sup> URO-OVA mice express the well-defined model antigen ovalbumin (OVA) as a “self” antigen on the urothelium and develop bladder inflammation upon adoptive transfer of OVA-specific T cells.<sup>33</sup> C57BL/6 mice were obtained from Charles River (Wilmington, MA, USA). All mice were housed in a pathogen-free facility at the University of Iowa Animal Care Facility under the conditions of constant humidity (30-70%) and temperature (20°C-26°C) with a 12:12-hour light/dark cycle. Mice were provided with irradiated Envigo Teklad laboratory diet no. 7913 (NIH-31 Modified Open Formula Mouse/Rat sterilizable diet) and filtered water from an Edstrom automatic watering system. Euthanasia was performed by exposing the animals to 100% CO<sub>2</sub> at a flow rate of 3 L/min until 1 minute after breathing stopped.

## METHOD DETAILS

### Human study

#### *Ethics statement*

This study was approved by the Institutional Review Board of The University of Tokyo Hospital [approval no. G10046]. All participants provided written informed consent before study enrollment.

#### *Sample preparation*

For patients with HIC, paired cold-cup biopsy samples, one from a Hunner lesion and one from a non-Hunner lesion (background mucosal area without Hunner lesion), were obtained at surgery, before hydrodistension. For patients with BCG cystitis, one cold-cup biopsy sample was obtained from a reddened mucosal flat lesion resembling a Hunner lesion (Figure S1) and subsequently diagnosed as BCG-related chronic cystitis and proven pathologically to be nonmalignant. All 13 participants in the BCG group had previously been diagnosed with primary intermediate- or high-risk NMIBC (including CIS, Ta, and T1 stages, classified according to the EAU guidelines<sup>27</sup>) and received a single intravesical injection of pirarubicin (20 mg) immediately after transurethral resection of the tumor and subsequent 8-week adjuvant intravesical instillations of BCG (Tokyo 172 strain, 80 mg; Nihon BCG, Tokyo, Japan) as NMIBC therapy. After BCG therapy, screening bladder biopsies were taken when patients showed irregular-looking and reddened bladder mucosal lesions at routine follow-up cystoscopy, with urine cytology class III (5 patients) or with negative cytology (8 patients), and examined pathologically for recurrent malignancy. Biopsy samples were sent to our department of pathology for histopathological examination or immediately frozen in liquid nitrogen and stored at -80°C for RNA extraction.

#### *RNA extraction*

Total RNA was extracted from frozen samples using NucleoSpin RNA (Macherey-Nagel, Düren, Germany). RNA was quantified on a NanoDrop 2000c Spectrophotometer (Thermo Fisher Scientific, San Jose, CA, USA), and the purity was measured using an RNA ScreenTape assay on a 2200 TapeStation (Agilent Technologies, Santa Clara, CA, USA). Quality assessment was performed using 2200 TapeStation Software (Agilent Technologies). The mean RNA integrity number equivalent (RINe) for the bladder biopsy samples used in this study was 7.1 (range, 5.2–8.9).

#### *RNA library preparation and NovaSeq sequencing*

Purified total RNA (10 ng) was resuspended in Clontech buffers for mRNA amplification using 5' template switching PCR with a SMART-Seq v4 Ultra Low Input RNA kit (Clontech, Palo Alto, CA, USA) according to the manufacturer's instructions. Amplified cDNA was fragmented and appended with dual-indexed barcodes using Nextera XT DNA Library Prep kits (Illumina, San Diego, CA, USA). The libraries were validated on an Agilent 4200 TapeStation system (Agilent, Santa Clara, CA, USA), pooled, and sequenced on an Illumina NovaSeq 6000 using a 2x150 paired-end (PE) configuration. Image analysis and base calling were conducted using NovaSeq Control Software. Raw sequence data (.BCL files) were converted into the FASTQ format and demultiplexed using Illumina bcl2fastq 2.20 software. One mismatch was allowed for index sequence identification.

#### *RNA-seq data processing*

Adaptor and low-quality portions, defined as sequences with an average Phred score < 10 in a 10-bp window, were removed from the raw reads. All remaining reads ≥ 36 bp in length were regarded as high-quality, clean data and used in downstream analyses. The clean PE reads were aligned to the University of California Santa Cruz (UCSC) human reference genome (hg19) using Genedata Profiler Genome ver. 11.0.8 (Genedata, Basel, Switzerland). Mapped reads were assembled using STAR ver. 2.5.3a by referring to gene structures described in the National Center for Biotechnology Information RefSeq. To quantify gene expression, fragments per kilobase of exon per million mapped fragments (FPKM) values for each gene model were calculated using the Genedata Profiler Genome.

### DEG analysis

RNA-seq data were analyzed using Genedata Analyst ver. 9.1.13 (Genedata, Basel, Switzerland) and Agilent Gene Spring software packages ver. 14.8 (Agilent Technologies). Genes for which the standard deviations of the FPKM scores were 0 or read counts were < 16 in every group were excluded as noisy data. A pseudocount of 0.0001 was added to the raw FPKM score for each gene prior to log<sub>2</sub> transformation. DEGs between each pair of the 3 groups (the Hunner lesions and non-Hunner lesion areas in HIC and BCG cystitis groups) were identified based on the log<sub>2</sub>-normalized FPKM scores by one-way analysis of variance (ANOVA) followed by Benjamini–Hochberg correction. HIC-specific DEGs were obtained by combining the genes that were significantly upregulated or significantly downregulated in both Hunner lesion and non-Hunner lesion area groups compared to the BCG cystitis group. HIC-specific were subjected to hierarchical clustering analysis with complete linkage and Pearson correlation analysis to obtain the overall transcriptional landscapes of HIC and BCG cystitis.

### GO and KEGG pathway enrichment analyses

Identified HIC-specific DEGs were subjected to GO/GO Slim analyses and KEGG pathway enrichment analysis to investigate the biological significance of DEGs characteristic of HIC using DAVID Bioinformatics Resources. GO terms and KEGG pathways with  $p < 0.05$  (Fisher's exact test) were considered significantly enriched.

### Histopathology and immunohistochemistry

All bladder tissue samples were fixed in formalin, embedded in paraffin, and used to prepare 4- $\mu$ m serial sections. Immunohistochemistry (IHC) was performed using a Ventana BenchMark XT autostainer (Ventana Medical Systems, Tucson, AZ, USA) as described previously.<sup>6,29</sup> Antibodies against the following proteins were obtained from the indicated suppliers: human CD3 (1:50, clone LN10, Novocastra, Newcastle upon Tyne, UK), CD4 (1:200, clone SP35, Roche, Basel, Switzerland), CD8 (prediluted, clone 4B11, Leica Biosystems, Buffalo Grove, IL, USA), CD20 (1:100, clone L26, Dako, Glostrup, Denmark), CD138 (prediluted; clone B-A38, Nichirei Bioscience, Tokyo, Japan), cGAS (MB21D1) (1:500, HPA031700, Sigma–Aldrich, St. Louis, MO, USA), cytokeratin (1:100, clone AE1+AE3, Dako, Glostrup, Denmark), FOXP3 (1:50, clone 236A/E7, Abcam, Cambridge, UK), IFN- $\gamma$  (1:200, ab218890, Abcam, Cambridge, UK), IL-17A (1:200, AF-317-NA, R&D Systems, Minneapolis, MN, USA), mast cell tryptase (MCT) (1:4000, clone AA1, Dako, Glostrup, Denmark), and STING (TMEM173) (1:50, HPA038116, Sigma–Aldrich, St. Louis, MO, USA). Appropriate controls for each antibody were run in parallel.

### Immunohistochemical quantification

Images of immunostained slides were digitized on a NanoZoomer Digital Pathology system (Hamamatsu Photonics, Hamamatsu, Japan), followed by digital immunohistochemical quantification using Tissue Studio ver. 3.5 (Definiens AG, Munich, Germany) as described previously.<sup>6,29</sup> The region of interest (ROI) was defined manually as the entire subepithelial area of each specimen. To determine the numbers of CD3-, CD4-, CD8-, CD20-, CD138-, FOXP-3, IL-17A-, and MCT-positive cells, a manual ROI-nucleus (positive vs. negative) analysis was performed as described in our previous studies,<sup>6,29</sup> and the IHC staining intensity thresholds were 0.3, 0.5, 0.5, 0.3, 0.5, 0.5, 0.6, and 0.8, respectively. To assess the degree of epithelial denudation, we performed manual ROI-marker area analysis as described previously.<sup>6</sup> The proportion of the cytokeratin-positive area in the ROI (whole-tissue sample area) was calculated and designated as the 'epithelium/specimen ratio (%)'. The densities of CD3-, CD4-, CD8-, CD20-, CD138-, FOXP-3, IL-17A-, and MCT-positive cells were calculated from the ratio of the cell count to the area of the ROI (cells/mm<sup>2</sup>). Due to the immunoreactivity in the stroma, the IHC staining intensity for cGAS, IFN- $\gamma$ , and STING was evaluated on a semi-quantitative manner as follows: negative, mild, moderate and strong, as described elsewhere.<sup>30</sup> Specimens with a negative or mild intensity were defined as having low immunoreactivity, and those with a moderate or strong intensity were defined as having high immunoreactivity. The sum of CD3-, CD20-, and CD138-positive cell counts was considered to represent the total lymphoplasmacytic cell count, accounting for the majority of subepithelial inflammatory infiltrates.

### Quantitative PCR

The mRNA expression for *IL2*, *IL4*, *IL6*, *IL10*, *IL12A/B*, *IL17A*, *IL22*, *IL23R*, *HIF1A*, *IFNA17*, *IFNB1*, *IFNG*, *TNF*, *TGFB1*, *TBX21*, *GATA3*, *RORC*, *CTLA4*, *CGAS*, and *STING1* was analyzed by real-time quantitative PCR. First-strand cDNA synthesis for target genes was performed by reverse transcription of 200 ng total RNA using a SuperScript VILO cDNA synthesis kit (Invitrogen, Carlsbad, CA, USA) in a 20- $\mu$ L reaction volume. Real-time quantitative PCR was performed using TaqMan® Universal Master Mix II, no UNG with TaqMan® Gene Expression Assays for target and internal control genes (Thermo Fisher Scientific, San Jose, CA, USA) (Table S9). The reaction volume of 10  $\mu$ L contained 2.25  $\mu$ L of sample genomic DNA, 2.5  $\mu$ L of TaqMan® Universal Master Mix II, no UNG, and 2.5  $\mu$ L of TaqMan® Gene Expression Assay for each gene. Quantitative PCR was performed on a BioMark Real-Time PCR System (Fluidigm, South San Francisco, CA, USA) under the following reaction conditions: 2 minutes at 50°C, 30 minutes at 70°C, and 10 minutes at 25°C for thermal mixing; 2 minutes at 50°C for the UNG reaction; 10 minutes at 95°C for Taq activation; and 40 cycles of 15 seconds at 95°C and 1 minute at 60°C. Standard curves were constructed using pMD20-hIPO8 plasmid vectors containing the target fragments. Amplification was performed in triplicate for each sample. The relative RNA load of each target gene was normalized against the copy number of the internal control RNA (*IPO8*).

## Generation of the mouse IFN- $\gamma$ DNA aptamer

### Reagents, chemicals and cell line

Reagents were purchased from standard suppliers and used without further purification. All DNA samples were synthesized by and purchased from Nihon Gene Research Laboratories Inc. (Sendai, Japan) or GeneDesign, Inc. (Osaka, Japan). Folding and annealing of the DNA aptamer were performed on a heat block at 95°C for 5 minutes, and then cooled on ice immediately. Dulbecco's phosphate-buffered saline (D-PBS) was obtained from Nacalai Tesque (Kyoto, Japan). Recombinant mouse IFN- $\gamma$  proteins (#50709-M02H, #50709-MNAH) were purchased from Sino Biological (Beijing, China). An Alexa Fluor 488-conjugated mouse anti-STAT1 (pY701) antibody (#612596) was purchased from BD Bioscience (Franklin Lakes, NJ, USA). The mouse derived L929 fibroblast cell line (#RCB1422 from RIKEN Bioresource Research Center Cell Bank, Tsukuba, Japan) was maintained according to the supplier's instructions. The unnatural base 7-(2-thienyl)imidazo[4,5-b]pyridine (Ds) was synthesized by and purchased from NARD Institute, Ltd. (Osaka, Japan). The oligonucleotide mIFN $\gamma$ 6-1mh was synthesized by and purchased from GeneDesign, Inc. (Osaka, Japan).

### Preparation for *in vitro* selection of the mouse IFN- $\gamma$ aptamer

Selection of the mouse IFN- $\gamma$  aptamer was performed using the SELEX method and our proprietary unnatural base pair technology as previously described.<sup>31,71,72</sup> A recombinant Fc-tagged mouse IFN- $\gamma$  protein was incubated with Protein G-Sepharose beads (BioVision, Palo Alto, CA, USA) in D-PBS supplemented with 0.02% Tween 20 (w/v) (PBS-T) at 4°C for 60 minutes for immobilization. After the incubation, the beads were washed with PBS-T three times and used for the selection process. For counterselection, normal human IgG (Wako Pure Chemical Industries, Osaka, Japan) was immobilized on Protein G-Sepharose beads by the same procedure. A previously constructed DNA library containing two unnatural hydrophobic base Ds at defined positions in the 42-natural-base randomized region was used for selection.<sup>74</sup>

### Isolation of mouse IFN- $\gamma$ binding sequences by SELEX

For DNA folding, the single-stranded DNA (ssDNA) pool was dissolved in D-PBS, denatured at 95°C for 5 minutes, and immediately cooled on ice. Then, an equivalent volume of PBS-T was added to the folded ssDNA solution. During the 1<sup>st</sup> selection round, mouse IFN- $\gamma$ -immobilized beads were incubated with the ssDNA solution at 4°C for 40 minutes. Then, the beads were washed with PBS-T three times and boiled at 95°C for 10 minutes to dissociate the mouse IFN- $\gamma$ -binding sequences. The eluted sequences were then amplified by PCR using AccuPrime DNA polymerase (Thermo Fisher Scientific, San Jose, CA, USA) as described previously.<sup>31</sup> During the 2<sup>nd</sup> to 6<sup>th</sup> selection rounds, as the counterselection, the ssDNA solution was incubated with normal human IgG-immobilized beads at 4°C for 60 minutes. Sequentially, as the positive selection process, the supernatant was incubated with mouse IFN- $\gamma$ -immobilized beads at 4°C for 10–20 minutes. Following the incubation, the beads were washed with PBS-T five times. The mouse IFN- $\gamma$ -binding sequences were dissociated from the beads and amplified by PCR using the same procedure used in the 1<sup>st</sup> selection round. To enrich the mouse IFN- $\gamma$ -binding sequences, these negative-positive selection cycles were repeated five times (for 6 rounds in total) (Table S10).

### Deep sequencing

To identify the sequences enriched through the SELEX selection process, we performed deep sequencing using an Ion PGM sequencer (Thermo Fisher Scientific, San Jose, CA, USA). After the six rounds of selection, the PCR products were purified with a QIAquick PCR purification kit (Qiagen, Hilden, Germany). The purified PCR products were ligated with adaptors using the Ion Fragment Library Kit, followed by Ion Sphere template preparation using the Ion OneTouch and Ion OneTouch ES System (Thermo Fisher Scientific) according to the manufacturer's instructions. Then, deep sequencing was performed using the Ion Sequencing Kit and Ion 314 Chip as described.<sup>31</sup> The obtained sequences were modified and optimized through a series of procedures including prediction of secondary structure, truncation and optimization of sequence. A wide range of modified sequences were analyzed for the binding affinity against mouse IFN- $\gamma$ . Eventually, two lead candidates were selected as the aptamer sequences based on the analytical results (Table S8).

### SPR analysis

The binding affinities of the two selected aptamer candidates were determined by SPR analysis using a Biacore T200 (GE Healthcare, Little Chalfont, UK) at 25°C. Each biotinylated aptamer was diluted to 25 nM in D-PBS, denatured at 95°C for 5 minutes, and immediately cooled on ice for DNA folding. Each folded aptamer was diluted to 0.5 nM in running buffer (D-PBS supplemented with 0.05% Nonidet-P40). Immobilization on a Sensor chip SA (GE Healthcare) was performed by injecting the aptamer solution for 8 minutes at a flow rate of 5  $\mu$ L/min in running buffer. Graded concentrations (1, 4, 16, 64 and 256 nM) of mouse IFN- $\gamma$  solution (diluted with running buffer) were injected onto the immobilized-DNA surface in kinetic injection mode. The measurement conditions were as follows: flow rate 100  $\mu$ L/min, contact time 180 seconds, and dissociation time 450 seconds. The sensor-gram was fitted to a single-kinetics model using BIAevaluation T200 software ver. 1.0 (GE Healthcare).

### Cell culture and IFN- $\gamma$ stimulation

The mouse fibroblast cell line L929 was cultured in minimal essential medium (MEM) (Nacalai Tesque, Kyoto, Japan) supplemented with 0.1 mM non-essential amino acids (NEAA) (Gibco BRL, Paisley, UK) and heat-inactivated 10% fetal bovine serum (Cat# F7524, Lot# BCBT3928, Sigma-Aldrich, Darmstadt, Germany). For the IFN- $\gamma$  signal neutralization test, L929 cells ( $1 \times 10^6$  cells/mL in Opti-MEM) were

stimulated with 2 ng/mL mouse IFN- $\gamma$  in the presence or absence of aptamers serially diluted with Opti-MEM at 37°C for 15 minutes. After the incubation, the cells were washed and subjected to flow cytometric analysis (Figure 6B).

#### Flow cytometric analysis

The neutralizing activity of aptamers against STAT1 phosphorylation was analyzed by flow cytometry. Cells were washed, resuspended in 0.5 mL 4% paraformaldehyde (Nacalai Tesque, Kyoto, Japan), incubated for 15 minutes at room temperature, centrifuged, resuspended in ice-cold methanol and incubated for 1 hour. Then the cells were washed twice with FACS buffer (DMEM containing 1% BSA), followed by incubation in 100  $\mu$ L FACS buffer containing an Alexa Fluor 488-conjugated mouse anti-STAT1 (pY701) antibody for 30 minutes at 4°C in the dark. The cells were resuspended in 0.5 mL FACS buffer, run on a flow cytometer (S3e, Bio-Rad, CA, USA) and visualized with *De Novo* software (FCS Express).

#### Pharmacokinetic study of intravesical instillation in mice

Female CD-1 mice were purchased from The Jackson Laboratory Japan, Inc. The mice (7 weeks old, weight range of 22–28 g) were anesthetized with isoflurane inhalation (4% in the induction phase and 2% in the maintenance phase). A 24-gauge intravenous catheter (Terumo Corporation, Tokyo, Japan) was then inserted into the bladder through the urethra, followed by injection of 100  $\mu$ L mIFN $\gamma$ 6-1mh in a D-PBS solution (10 nmol/bladder) into the bladder. After intravesical instillation, the mice were maintained under anesthesia for 10 minutes. Blood samples were collected from the postcaval vein at 10 minutes, 3 hours and 24 hours after the intravesical administration. For plasma sample preparation, the whole-blood samples were collected into a tube with EDTA-2K (final conc. 1 mg/mL), followed by centrifugation at 12,000 $\times$ g and 4°C for 15 minutes. The plasma in the upper layer were then collected and stored at –30°C until measurement. Following blood sampling, bladders were collected after euthanasia by exsanguination. The bladder samples were incised to expose the inside of the bladder, washed three times with PBS, and weighed. Then, the bladders were put into tubes with 500  $\mu$ L DNAzol® Direct (Molecular Research Center, Inc., OH, US) and incubated for 15 minutes at room temperature to lyse the tissues. The tubes were vortexed and stored at –30°C until measurement. To measure the aptamer concentration in serum, plasma and bladder extracts, quantitative PCR was performed with KOD SYBR qPCR mix (#QKD-201, TOYOBO, Osaka, Japan) on a CFX connect instrument (Bio-Rad, CA, US) according to the manufacturer's instructions. Briefly, serum, plasma or bladder samples were diluted 100-fold with nuclease-free water. For standard curve construction, mIFN $\gamma$ 6-1mh was serially diluted with EASY Dilution (#9160, Takara Bio, Shiga, Japan) and spiked in serum, plasma or bladder extract samples from a nontreated mouse. The 20- $\mu$ L PCR mixture included 2  $\mu$ L diluted sample, 0.4  $\mu$ M forward primer (5'-GGCCGGTACCCGAACACAGTTTATAGTTGACTA-3') and 0.4  $\mu$ M reverse primer (5'-CGCTTCGCGGGCCAGACCCTGC-3'). Quantitative PCR was performed at 95°C for 2 minutes, followed by 40 cycles at 95°C for 10 seconds, 52°C for 10 seconds and 68°C for 30 seconds.

## URO-OVA mouse experiments

#### Ethics statement

All animal experiments were approved by the University of Iowa Animal Care and Use Committee [approval no. 1308153] and conducted according to the National Institutes of Health *Guide for the Care and Use of Laboratory Animals*.

#### Induction of HIC-like bladder inflammation in URO-OVA mice

As previously described,<sup>32</sup> to generate OVA-specific lymphocytes for the induction of HIC-like cystitis in URO-OVA mice, C57BL/6 mice (female, 7–8 weeks old) were subcutaneously immunized with 100  $\mu$ g OVA (Sigma-Aldrich, St. Louis, MO, USA) emulsified with complete Freund's adjuvant (CFA, Sigma-Aldrich). Fourteen days later, the OVA-immunized mice were euthanized, and the spleens were removed under sterile conditions, minced, filtered through a fine nylon mesh, placed in ACK lysis buffer (0.15 M NH<sub>4</sub>Cl, 1.0 mM KHCO<sub>3</sub>, and 0.1 mM Na<sub>2</sub>EDTA, pH 7.4), washed with RPMI-1640 medium, and then subjected to Ficoll-Paque gradient centrifugation to fractionate the splenocytes. The viability of the fractionated splenocytes was measured by trypan blue exclusion and confirmed to exceed 90%. URO-OVA mice (female, 7–8 weeks old) were then anesthetized through intraperitoneal (i.p.) injection of a solution of ketamine (87.5 mg/kg) and xylazine (12.5 mg/kg), followed by intravenous (i.v.) injection of OVA-primed C57BL/6 splenocytes (5  $\times$  10<sup>7</sup> cells in 100  $\mu$ L PBS per mouse) via the orbital sinus. Sex- and age- matched URO-OVA mice that did not receive splenocyte transfer (i.e., cystitis-uninduced) served as control.

#### Intravesical instillation of mIFN $\gamma$ 6-1mh

The URO-OVA mice were randomly divided into three groups: the cystitis-induced and mIFN $\gamma$ 6-1mh-treated group, cystitis-induced and PBS-treated group, and cystitis-uninduced control group (non-treated or PBS-treated). For the treatment groups, mice were anesthetized with ketamine/xylazine, and the bladder was catheterized via the urethra with a 24-gauge, 3/4" long plastic intravenous cannula. mIFN $\gamma$ 6-1mh (10 nmol in 100  $\mu$ L PBS) or PBS (100  $\mu$ L) was intravesically instilled into the bladder and retained for 1 hour. In an initial experiment, the treatment was administered every other day for a total of 12 times starting immediately after cystitis induction on day 0. In a subsequent experiment, the treatment was administered for a total of 3 times on days 1, 4 and 7 after cystitis induction. The treatment dose of mIFN $\gamma$ 6-1mh was determined based on the results from our previous study for human alopecia areata, a CD8-positive T cell-dependent autoimmune hair loss disorder.<sup>75</sup> We observed that intradermal local treatment with 4.5 pmol of TAGX-0003 (a human anti-IFN- $\gamma$  DNA aptamer, K<sub>D</sub>=33.0 pM) every other day sufficiently suppressed the levels of IFN- $\gamma$  expression at the affected sites and ameliorated the hair loss in a humanized mouse model of alopecia areata.<sup>75</sup> Based on these results and the differences in the K<sub>D</sub> values between the TAGX-0003 and mIFN $\gamma$ -1mh (K<sub>D</sub>=2.47 nM), alternate-day administration of 10 nmol/bladder of mIFN $\gamma$ 6-1mh was determined as the treatment protocol of this study.

### *Pelvic nociception analysis*

As previously described,<sup>32</sup> the sensory threshold of pelvic nociception was analyzed using an electronic von Frey anesthesiometer (VFA, IITC Inc. Life Science, Woodland Hills, CA, USA). In an initial experiment, this was performed before cystitis induction and on days 8, 15 and 22 after cystitis induction. In a subsequent experiment, this was performed before cystitis induction and on days 8, 14 and 21 after cystitis induction. Briefly, mice were kept in individual Plexiglas chambers with a stainless-steel wire grid floor. After acclimation, the semirigid filament of the evaluator was advanced perpendicularly into the skin covering the lower abdominal area in the general vicinity of the bladder until the subject showed a positive response defined as sharp abdominal retraction, brisk licking or scratching of the stimulated area, or jumping. The maximum force applied by the VFA filament that caused a positive behavioral response was recorded as the measured sensory threshold. In total, five trials were completed for each subject, with a 30-second interval allowed between measurements. For the five threshold values obtained for each subject, the highest and lowest values were excluded, and the three middle values were averaged to assign each subject a sensory threshold.

### *Voiding behavior analysis*

As previously described,<sup>32</sup> voiding behaviors were analyzed using computer-interfaced micturition cages (Columbus Instruments, Columbus, OH, USA). In an initial experiment, this was performed before cystitis induction and at weeks 1, 2 and 3 after cystitis induction. In a subsequent experiment, this was performed before cystitis induction and at weeks 1 and 2 after cystitis induction. Briefly, mice were kept in individual cages for 24 hours with a 12:12-hour light/dark cycle. Mice had free access to drinking water but were fasted from solid food consumption to prevent feces from interfering with the measurement of urine output. Urinary frequency and voided volume were recorded using Oxymax software (Columbus Instruments, Columbus, OH, USA).

### *Bladder histology*

At the end of experiments, the bladders were collected from all URO-OVA mice after euthanasia. In an initial experiment, URO-OVA cystitis mice were euthanized two days after the last intravesical treatment (day 24). Cystitis-uninduced control URO-OVA mice were euthanized one day later (day 25). In a subsequent experiment, all URO-OVA were euthanized fourteen days after the last intravesical treatment (day 21). The bladders were then collected, fixed in 4% paraformaldehyde, and processed for paraffin embedment, section preparation, H&E staining, and imaging as previously described.<sup>32</sup> Bladder inflammation was scored based on the degrees of inflammatory cell infiltration and stromal inflammatory changes, such as edema and vascularity, as previously described (Grade 0: none or minimal inflammatory cell infiltration with few stromal changes; Grade 1: mild infiltration with mild stromal changes; Grade 2: moderate infiltration with moderate stromal changes; and Grade 3: moderate to severe infiltration with severe stromal changes).<sup>32</sup>

### *Reverse transcription polymerase chain reaction (RT-PCR) for bladder gene expression*

As previously described,<sup>32</sup> total RNA was extracted from the bladder using the Qiagen RNeasy Mini Kit (Qiagen, Valencia, CA, USA), and cDNA was synthesized using Invitrogen SuperScript III Reverse Transcriptase (Invitrogen, Carlsbad, CA, USA) and oligo (dT)<sub>20</sub>. PCR amplification of cDNA products was performed using Taq DNA polymerase (New England Biolabs, Ipswich, MA, USA) and the following sequence-specific primer pairs for *Ifng*, *Tnf*, *Tac1*, *Ngf* and glyceraldehyde-3-phosphate dehydrogenase (*Gapdh*). Based on the PCR kinetics previously established in our laboratory, *Gapdh* was amplified for 25 cycles, and the other molecules were amplified for 40 cycles. The amplified PCR products were run on 1% agarose gels, stained with SYBR Safe DNA gel stain (Invitrogen), photographed with a Gel Doc EZ Imager (Bio-Rad Laboratories, Hercules, CA, USA). The PCR band density of each gene was quantified by digital image analysis using ImageJ software (USA National Institutes of Health: <http://rsb.info.nih.gov/ij>) and normalized to that of *Gapdh* from the same sample.

### *Aptamer concentration in the serum*

At the time of euthanasia (two days after the last intravesical treatment), serum samples were collected, and the aptamer concentration was measured by quantitative PCR analysis. The further details of quantitative PCR method is described in the section of '[pharmacokinetic study of intravesical instillation in mice](#)'.

## **QUANTIFICATION AND STATISTICAL ANALYSIS**

In DEG analysis of the RNA-seq data, the statistical significance of differences in gene expression was evaluated at a false discovery rate (FDR)  $\leq 0.05$ . Group-specific DEGs were detected by generating a Venn diagram from the DEGs between each pair of groups, as identified by multiple pairwise comparisons among the 3 groups using the Tukey–Kramer test. The statistical significance of the Tukey–Kramer test was evaluated at an FDR  $\leq 0.05$ . Otherwise in human study, multiple and pairwise comparisons of continuous variables were conducted using the Steel–Dwass test and Wilcoxon rank–sum test, respectively. Fisher's exact test was used for comparisons of categorical variables. In URO-OVA mouse experiments, data were analyzed using GraphPad Prism software version 8 and presented as means  $\pm$  SD for bladder gene expression and sensory threshold or as mean  $\pm$  SE for urinary frequency. Data were compared using Student's t-test for two groups or ANOVA for multiple groups.

A P value  $< 0.05$  was considered statistically significant.